Final Technical Report of NASA Innovative Advanced Concepts (NIAC) Phase I, Grant NNX15AL89G

APERTURE, A LARGE TELESCOPE USING MAGNETOSTRICTION FOR POST DEPLOYMENT CORRECTIONS

M. P. Ulmer*[1], V. L. Coverstone[2], J. Cao[1], Y.-W. Chung[1], M.-C. Corbineau[2], A. Case[2], B. Murchison[2], C. Lorenz[2], G. Luo[2], J. Pekosh[2], J. Sepulveda[2], A. Schneider[1], X. Yan[1] and S. Ye[1]

[1]Northwestern University
[2]University of Illinois at Urbana-Champaign

March 4, 2016

*Prof., Dept of Physics and Astronomy at Northwestern University, mailing address: 2131 Tech Drive, Dearborn Observatory, Dept. of Physics and Astronomy, Northwestern Univ., Evanston, IL 60208-2900, phone: (847)-491-5633, email: m-ulmer2@northwestern.edu

Contents

1 Introduction 6

2 Need for the Concept 6

3 Potential Mission and Benefits to NASA 7

4 Summary of Phase I Goals, Objectives and Tasks 8

5 Summary of Research 10

5.1 Study of the Feasibility of Shape Corrections Using Magnetostriction 10

5.1.1 Magnetostriction, General 11

5.1.2 Magnetic Smart Materials and Applications 11

5.1.3 Selection of appropriate Magnetic Smart Materials (MSM) 11

5.1.4 Magnets for Correction 12

5.2 Deployment study 13

5.2.1 Design of the Stowed Primary Mirror Membrane 14

5.2.2 Determination of a Condition Before Micro-Yield 17

5.2.3 Deployment Mechanism 20

5.3 Operation and Characteristics of the Post Deployment Shape Correcting System 22

5.3.1 Baseline Values of the Parameters 23

5.3.2 Diameter of the Primary Mirror 25

5.3.3 Mission Lifetime 25

5.3.4 Number of Cycles of the Magnet Battery 26

5.3.5 Number of Cycles of the Main Battery 27

5.3.6 Percentage of the Main Battery Allocated to Charge the Magnet 27

5.3.7 Size of the Magnet Battery 28

5.3.8 Size of the Solar Panels 28

5.3.9 Surface of the Magnet 29

5.3.10 Time Allocated to Each Location 29

5.3.11 Number of Magnets 29

5.3.12 Summary 32

5.4 Preliminary APERTURE Design 35

5.4.1 Magnetic Smart Material and Substrate 35

5.4.2 Magnetic Write Head 35

5.4.3 Operation and Characteristics of the Post Deployment Shape Correcting System 36

5.4.4 Stowed Configuration and Deployment Mechanism 36

5.4.5 Post Deployment Figure Assessment and Feedback 37
5.5 Concept Verification Testing 37
6 Work Plan for Phase I 39
6.1 Tall Poles for Phase II 39
6.2 Task Breakdown 40
7 Summary and Conclusions 44
8 Publications, Conferences and Patents 45
8.1 Publications and Conferences 45
8.2 Patents 45
9 Contacts with experts in at NASA, NIST and Northrup Grumman 46
10 Acknowledgments 46
11 References 47

List of Figures

1 APERTURE concept
2 MOIRE concept
3 Schedule for Phase I
4 Schematic of the experimental setup to measure displacement due to magnetostriction on a thick glass substrate coated with Terfenol-D
5 Experimental setup to measure displacement due to magnetostriction on a thick glass substrate coated with Terfenol-D
6 Experimental results for a 2-D scanning glass sample coated with MSMs
7 Payload Static Envelop, 5-m diam by 19.1-m Composite Fairing, Delta IV Heavy
8 Umbrella design, circular shapes
9 Umbrella design, top section
10 Number of petals for different values of the diameter
11 Minimal radius of curvature for different values of the diameter
12 Umbrella design, 3D-folded mirror
13 Strain-stress curves for Galfenol and Kapton®
14 Strain-stress approximated for Galfenol
15 Strain-stress approximated for Kapton®
16 Radius of curvature before micro-yield for Kapton® with different values of the deflection
17 APERTURE deployment (conceptual view)
18 Flexible reflector
19 Deployment of the self-deployable shell reflector
20 Solar array output power versus solar range using polynomials method
21 Diameter of the Primary Mirror
22 Depth-of-discharge versus cycle life
23 Mission Lifetime
24 Number of Cycles of the Magnet Battery
25 Number of Cycles of the Main Battery
26 Percentage of the Main Battery Allocated to the Magnet
27 Size of the Magnet Battery
28 Size of the Solar Panels
29 Surface of the Magnet
30 Time Allocated to Each Location
31 Number of Magnets
32 Quantification of the impact of different variables (1/2)
33 Quantification of the impact of different variables (2/2)
34 Two types of magnetic write head designs
35 Regularly spaced grid and distorted wavefront
36 Test geometry diagram

List of Tables

1 MSM Material Properties
2 Radius of curvature before micro-yield for different materials and different values of the thickness (deflection = $1\mu m$)
3 Characteristics of the two selected deployment designs
4 Impact of different parameters over the time required to correct the mirror
5 Alternative design
6 Shack-Hartmann Test Components

1 Introduction

The goal of this Phase I study is to establish that the APERTURE mission presents a feasible approach toward the reality of deployable diffraction-limited ultraviolet-visible (UV-Vis) mirrors of 16-m diameter or larger. APERTURE, which stands for "A Precise Extremely large Reflective space Telescope Using Reconfigurable Elements", uses a Magnetic Smart Material (MSM) to apply figure corrections to extremely large (≥16-m) deployable reflective optics. The first step of the deployment will utilize an umbrella-like structure and MSM to achieve a parabolic shape for the optics. The inside of the umbrella will be the reflective surface, while the outside will be coated in MSM. A magnetic write head will move to different locations on the MSM coated side to manipulate the MSM, changing the shape of the optics and eliminating any deviation from the desired final shape. Figure 1 depicts the concept of APERTURE: the write head (in dark gold color) moves along the curved arm, while the curved arm rotates about the center axis.

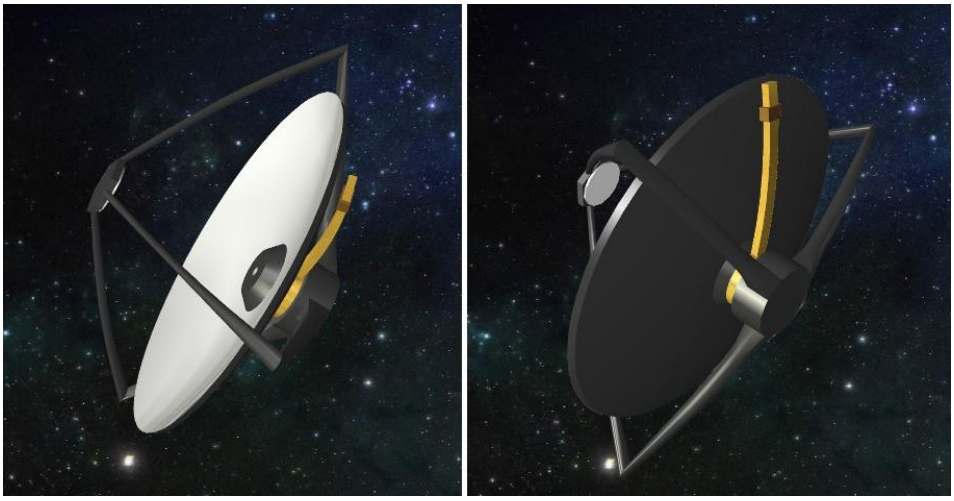

Figure 1 APERTURE concept. For simplicity only one write head is shown. The QR code leads to an animation depicting the concept found here link to video

2 Need for the Concept

The desire for larger space telescopes is ever present. The UV-Vis Hubble Space Telescope (HST) and the near-infrared (NIR) James Webb Space Telescope (JWST) have a diameter of 2.4 m and 6.5 m respectively, and the Advanced Technology Large-Aperture Space Telescope (ATLAST) concept has a desired maximum diameter of 16 m [1] and requires the 10-m baseline fairing of the now canceled Ares V heavy lift vehicle [2]. Therefore, even if rocket fairings are made larger, the astronomers' desire for larger apertures will surely outstrip the ability of rocket fairings to accommodate these larger apertures.

In response to the desire for greater than 16-m diameter mirrors, deployable mirrors are the logical choice. Within this category there are segmented mirrors, e.g. JWST, and a preliminary conservative approach of scaling up JWST by unfolding rigid segments

yields an about 12-m diameter design [3]. Conversely, for deployable membrane optics, the limiting diameter is more than 16 m. The problem with any membrane-like mirror, however, is that they have yet to achieve figure better those acceptable for S, Ku and Ka-band wavelengths (respectively ≈ 150 mm, ≈ 20 mm, ≈ 11 mm), such as the Tracking and Data Relay Satellites (TDRS) [4] or the AstroMesh design [5]. If one assumes a Strelh ratio of 90%, then the Ka-band wavelength corresponds to a figure Root Mean Square (RMS) error of about 11 mm/20. Since APERTURE is meant to be used for UV-Vis observation, a similar Strelh ratio would lead to a RMS of 400 nm/20 (or better for the deep UV). Therefore if a deployed membrane mirror is to be employed, then post-deployment corrections will need to be applied within the context of current designs.

The general concept of membrane and deployable mirrors associated with electrostatic or piezoelectric control has been studied in the past. A big disadvantage is that wires must be attached to every point on the mirror for which actuator control is needed, and so far the ability to provide post deployment figure corrections to the level of λ/20 in the visible has eluded the space community. Previous work has been done using polyvinylidene fluoride (PVDF) actuators for surface control on a flexible Kapton® reflector by Jeffrey R. Hill, et al. [6]. Their experiment concluded that a feasible RMS surface error between ≈100 μm and 400 μm is obtainable depending on the initial configuration of the reflector. While a surface error of this scale is accurate enough for long (≈ 1 mm) wavelength reflectors, a reflector operating in the UV wavelength range requires a surface error of at most 10 nm. Therefore, a UV-Vis space reflector requires an alternate method of post deployment correction from piezoelectric actuators. What is new about our approach is that it uses moving magnetic write heads to modify the mirror figure *without attachment* to the mirror.

There has also been recent excitement generated by a concept funded by DARPA [7]. The DARPA approach uses diffraction from the membrane surface as illustrated on Figure 2, whereas our concept uses the more classic concept of reflection from the mirror surface. Using the proposed method, high quality images could be made from the extremely large optics, opening up a wide variety of opportunities for new discoveries. This will be a game changing technology for astronomy, as astronomy is always light limited.

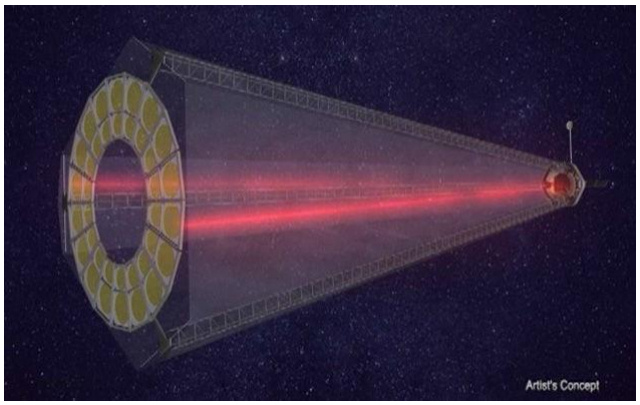

Figure 2 MOIRE diffraction telescope concept (DARPA project)

3 Potential Mission and Benefits to NASA

As noted in the previous section, in contrast to using magnetostriction, all current space

mirrors rely on the piezoelectric effect which then requires that actuators be attached to the mirror and that wires need to be attached to the actuators. The piezoelectric approach is the baseline for the Advanced Technology Large-Aperture Space Telescope (ATLAS-T) mission and the APERTURE concept presents great potential benefits to this future mission. A major benefit of our approach of using a flexible mirror rather than many combined rigid segments, is that the design can be expanded well beyond the current 16-m diameter (the proposed maximum diameter) of ATLAST [1]. Indeed, provided that the membrane is thin enough, we can apply our umbrella design to larger diameters (see 5.2.1). Larger mirrors with commensurate figure quality open up a larger discovery space. Also, the maturing of the technology proposed here would lead, by extension, to even more technological challenges such as the Terrestrial Planet Finder [8]. In addition, the ATLAS-T concept, which required the 10-m baseline fairing of the now canceled Ares V heavy lift vehicle [2], needs the future modified Space Launch System (SLS) while we proved in our Phase I that a membrane mirror can fit into the existing Delta Heavy IV rocket fairing without producing structural micro-yield.

The overall goal of the Phases I and II is to produce a proof that the technology concept underlying APERTURE has enough merit to follow through with aggressive funding to bring the idea to TRL 6. Due to the modest funding available in Phase I and II, however, we propose to address what we consider the two tallest poles of the concept. We plan therefore in Phase II to demonstrate that these overall issues of the concept are surmountable, and thus that a significant funding and manpower push to carry on further work is warranted. Phase I was entirely a paper study to design experiments and extensive (beyond those in Phase I) computations to be carried out in Phase II. The Phase I also helped us identify many of the problems our concept faces. We give the resulting tall pole list in 6.1. As an aside, it should be noted that although the focus of this project is the comparison to the NASA ATLAS-T astronomical telescope project, NASA's Earth Observing Office is equally interested in large aperture telescopes.

4 Summary of Phase I Goals, Objectives and Tasks

To develop this technology, several aspects were explored via a literature search, calculations, and simulations:

- Determine materials that are both flexible enough to be folded up and yet rigid enough to maintain this figure with fine post-deployment adjustments.
- Determine the best magnetic material to coat the mirror, which is flexible and does not distort the figure beyond the possible correction range.
- Determine a design for the write head system that has a strong enough magnetic field to affect the desired changes on the required length scales across the mirror.
- Determine an approach to vary the magnetic field strength and direction, e.g., two permanent pole magnets whose orientation and distance from the mirror change the magnet field, versus an electromagnet which varies the magnetic field strength by changing the current.
- Determine how to coat large monolithic membranes with the requisite material, or how to stitch together segments that are small enough to coat easily.
- Determine how to characterize the mirror figure in orbit.
- Determine how to ensure that the figure can hold its shape for times longer than

the time required to bring the figure into shape.
- Select potential deployment mechanisms that can lead to an accurate post-deployment shape which could then be corrected using magnetic write heads.

Given the above requirements, major tasks are to be carried out via literature search, calculations, and simulations, and are organized as follows:

Task 1: Select a set of materials, characterize them, and define thicknesses necessary for a test in Phase II
Major Task 1 will be led by Ulmer (overall organization plus direct supervision for the ray tracing simulations) along with input from key personnel, Chung (Materials with a focus on magnetic properties of them) and Cao (Mechanical Engineering and deflection vs stress).

Task 1.1: Find a polymer thick enough to not be too floppy but thin enough to be correctable over the smallest length scales. Milestone due in month 3.
Task 1.2: Find a magnetic hard material thick enough to hold in the field, but thin enough to be flexible. Milestone due in month 4.
Task 1.3: Find a MSM material that is thin enough to be flexible but strong enough to make the shape changes needed over the requisite length scale. Milestone due in month 5.
Task 1.4: Determine an adhesion process among all the layers. Milestone due in month 5.
Task 1.5: Evaluate Coefficient of Thermal Expansion (CTE) issues of survivability during transport and launch. Milestone due in month 6.
Task 1.6: Determine the length scale for figure correction need to be made via ray tracing and feedback this information to the properties of the reflecting layer, the polymer, the MSM, and magnetic hard material. Milestone due in month 6.
Task 1.7: Determine if the MSM can also be a magnetic hard material, and if so, what should it be. Milestone due in month 3.
Task 1.8: Match the annealing temperature to substrate such that annealing, if necessary, will not damage the substrate. Milestone due in month 4.
Task 1.9: Determine the extent, if any, that out-gassing will affect the shape and or surface once deployed in space. Milestone due in month 6.

Task 2: Develop a process for large scale replication of 200 m² reflective surface
Replication technology is an important but not unique (for this concept, e.g. the current ATLAST 16 m design). If a convincingly affordable design which matches with the MSM concept cannot be devised, the other parts of the design will not matter. Furthermore, deployment design will be based on replication design. Feedback between the substrate fabrication techniques and the deployment will also be considered. Major Task 1 will be joint with the personnel at NU (Ulmer, replication; Chug, materials), and UIUC (Coverstone, deployment). Milestone due by 3rd month.

Task 3: Produce a preliminary design of the stowage and deployment
Stowage and deployment designs need to take into account both how each segment and monolithic membrane is formed, as well as the materials used. A preliminary design will be carried out in Phase I. Major Tasks 3-4 will be primarily carried out by UIUC: Coverstone is the key personnel, with input on deflections and write head capabilities (Task 3) from Chung and Cao. Milestone due in month 6.

Task 4: Produce a preliminary design of the magnetic write head system
The magnetic write head, and how it is to be moved around, requires a preliminary design and a preliminary determination of the requirements of the write head coupled with the deployment design. The deployment depends on the design of the magnetic write head because if, for instance, the magnet is moved around on some kind of wire, the deployment of the wire can be critical. This item is an engineering challenge as it can cause limitation on the overall design. In the case of the wire, for example, the use of jets would be inappropriate because of contamination and because the design would have an expendable component which is undesirable for long term operability. This task also covers the issue of the placement of the magnet relative to the surface. Milestone due in month 7.

Task 5: Synthesize an overall preliminary design
Major tasks 5 and 6 will be performed by all personnel. Milestone due in month 8.

Task 6: Reporting and meeting
Progress reports will be written every two months, as well as a final report for Phase I at the end of month 9. Additionally, PI Melville P. Ulmer will attend the two program meetings required, namely the two-day NIAC orientation meeting and the three-day NIAC symposium. The two meetings are not specified in the project schedule given that the dates and locations are to be determined.

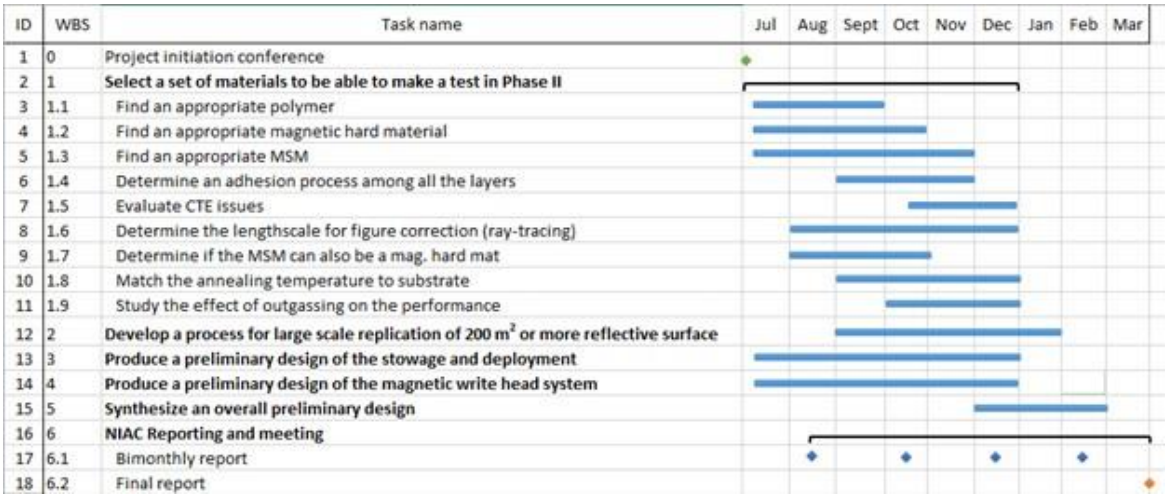

Figure 3 Schedule for Phase I

Below follows the summary of what we learned in Phase I.

5 Summary of Research

5.1 Study of the Feasibility of Shape Corrections Using Magnetostriction

The amount of literature on this topic is so large that we will not give a comprehensive review of MSMs and magnets. Rather we give a few references and make a few key points about the phenomenon of magnetostriction, the methods of applying MSMs via sputtering or plating, and the structure of the MSMs films which can either be a single layer of a

homogeneous material or a sandwich of multilayers.

5.1.1 Magnetostriction, General

The general effect is that any ferromagnetic material will expand or contract in the presence of a magnetic field. The effect is called magnetostriction and has been known since 1842 with work done by Joule and recently others [9, 10]. Both expansion and contraction are possible, see for example [10]. Magnetostrictive thin films have so many interesting and complex properties, that they have been studied extensively; see, for example the references found in [11, 12, 13].

5.1.2 Magnetic Smart Materials and Applications

The magnetostrictive material Terfenol-D was invented in the 1960's by the Naval Ordnance Lab [14] and exhibited giant magnetostriction, on the order of δL/L as high as 0.2%. The maximum saturation magnetic fields are about 0.5 T. Much research has been devoted to understanding the basic principles underlying the behavior of giant magnetostriction. There are now a range of materials to select from depending on parameters such as the optimal annealing temperature, applicable coating method (e.g. electroplate versus sputter deposit), and how much magnetostriction is desired. Besides Tefenol-D, other materials such as Tb-Fe or Fe-Ga (Galfenol) exhibit magnetostrictive properties [15, 16], as do multilayers such as $Tb_{40}Fe_{60}Fe_{50}Co_{50}$ [17] and $BaFe_{12}O_{19} - CoNiP$Ba [18]. A few of many applications are described in [19]. They are mostly used for actuation but micro-electro mechanical systems (MEMS) have also been proposed, e.g. [18]. The application that we are proposing is different from these, as an MSM film will instead be used to correct a deployed membrane optic, where ``membrane'' is defined to be flexible enough to be folded up in pre-deployment as well as thin enough to be correctable by the strains induced in MSMs via a magnetic field.

5.1.3 Selection of appropriate Magnetic Smart Materials (MSM)

Two options have been identified for the MSM: (a) Terfenol-D, which requires a high magnetic remanence layer of say, NiCo as well; (b) V-Permadur, which has a high remanence and thus holds very well the magnetic field. An alternative solution is to use Galfenol, which is similar to Terfenol-D, but more pliable. In addition to the reaction magnitude to magnetic field, remanence and flexibility, another parameter that needs to be taken into account is the Coefficient of Thermal Expansion (CTE). Table 1 summarizes some properties of MSMs mentioned above along with the substrate and reflective material.

Table 1MSM Material Properties

Material	Young's Modulus (GPa)	Poisson Ratio	CTE (ppm/°C)
Terfenol-D	216.9 (varies according to applied magnetic field)	0.5	12
Galfenol	75	0.3	11.7

Vanadium-Permendur	207	-	9.50 (25 - 200˚C)
Kapton®	2.5	0.34 (at 23˚C)	20 (for -14 to 38˚C)
Al-2014 T6	72.4	0.33	23

5.1.4 Magnets for Correction

The maximum required magnetic field is about 0.5 T as this is the saturation magnetic field. These fields can be produced either via permanent rare-earth magnets or electromagnets. Permanent magnets [20] of acceptable size (volumes of ≈ 2 cm^3) can produce the required field as can electromagnets of about 10 cm^3 with acceptably low power levels of less than a few Watts. Based on the experimental result from Wang et al. [12] [21] (see figures 4, 5, 6 from this work), about 1 μm of deflection can be obtained from a 100 μm thick glass substrate (Young's modulus ≈ 80 GPa) over a 20 mm x 5 mm strip under a magnetic field of 0.1 T. Wang et al. have developed an analytic model which produced results that match closely with the experimental result. Using this model, it can be estimated that if a Kapton® substrate is used under the same conditions, deflections of about 40 μm can be obtained. By reducing the thickness to 25 μm, the size of deformations possible rises inversely as the square of the thickness to a net deformation of over 600 μm. Furthermore the magnetic field strength can be raised to the saturation value to produce another factor of ≈ 0.5. Hence it is plausible that corrections of ≈ 300 μm are possible in candidate membrane materials.

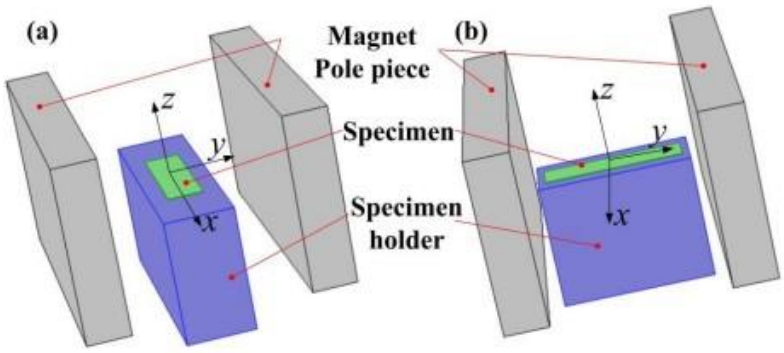

Figure 4 Schematic of experimental setup for measurements of surface profile on 5 mm wide by 20 mm long pieces. (a) Magnetic field perpendicular to the long direction of the specimen; (b) Magnetic field parallel to the long direction of the specimen.

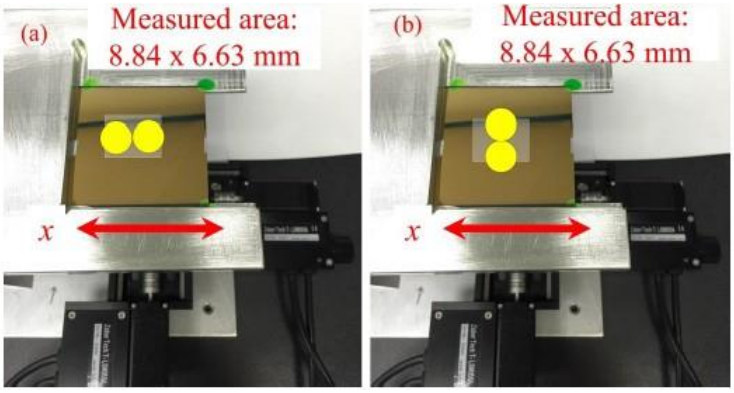

Figure 5 (a) Schematic showing locations of magnets and measurement area with 3 corners of a rectangular sample (50 x 50 mm) fixed on the stage; (b) rotate the magnets by 90°.

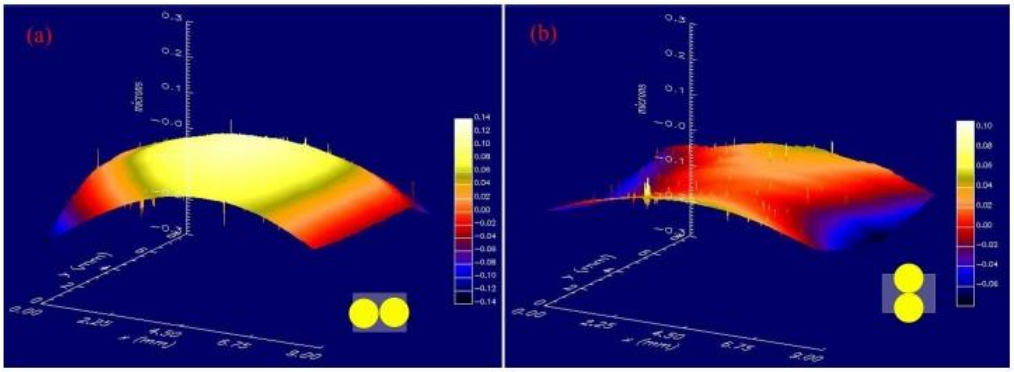

Figure 6 (a) The deformation of the coated glass sample with 3 corners fixed as shown in the configuration of magnets in Figure 5 (a); (b) the deformation of the coated glass sample with 3 corners fixed as shown in the configuration of magnets in Figure 5 (b).

5.2 Deployment study

APERTURE's deployment design assumes the utilization of a Delta IV Heavy rocket which can carry a payload with a diameter up to 4.6 m and a height less than 17 m. For simplicity, only solid monolithic designs will be considered for the secondary mirror and, given the dimensions of the rocket fairing, its diameter is constrained to be less than 4.6 m. Initially, both segmented and monolithic approaches were considered for the deployment study. Segmented approaches, like the one used for JWST, are usually associated with piezo-actuators that are responsible for aligning the segments after deployment. This is in contradiction with the original purpose of APERTURE which is to avoid the utilization of piezo-actuators. Moreover, JWST uses 18 hexagonal segments with two foldable panels but for primary mirrors as large as APERTURE's, segments of the size used for JWST would not fit.

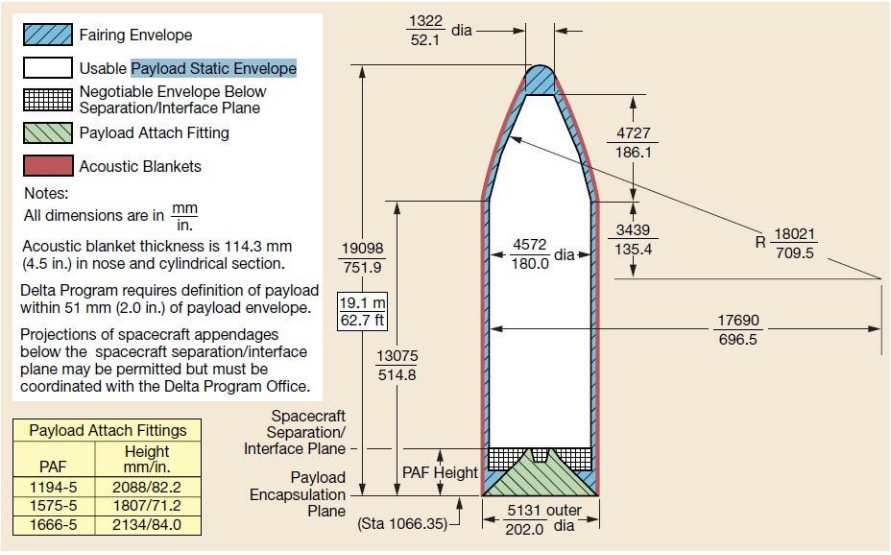

Figure 7 Payload Static Envelope, 5-m diameter by 19.1-m Composite Fairing, Delta IV Heavy [22].

Given the dimensions of the desired rocket fairing, if the mirror is monolithic then it needs to be flexible. Moreover, the thinner a membrane is, the easier it is to make corrections

with a magnetic write head. However, if the membrane is too thin, it would not be able to hold the parabolic shape. Therefore, some stiffeners are needed. Another parameter that needs to be taken into account in the calculation of the thickness of the membrane is its extreme susceptibility to micro-yield (microscopic plastic deformation). It is necessary to make sure that the membrane can be folded within the rocket fairing without being damaged.

5.2.1 Design of the Stowed Primary Mirror Membrane

The first shape that has been considered is the umbrella design. This shape has been studied by Enders et al. [23], however, there is a limitation due to the way the section is generated since it is based on circles, and for large apertures this strategy is not applicable, as shown on Figure 8. In this report we present a variation of the method described by Enders et al.; instead of generating the section using circles we use Eq.1 and Eq.2 where $2p$ is the number of petals and $r_0 + \rho$ is the maximal radius of the stowed membrane.

$$\theta = t + \cos^4(pt) \tag{1}$$

$$r = r_0 + \rho \cos^4(pt) \tag{2}$$

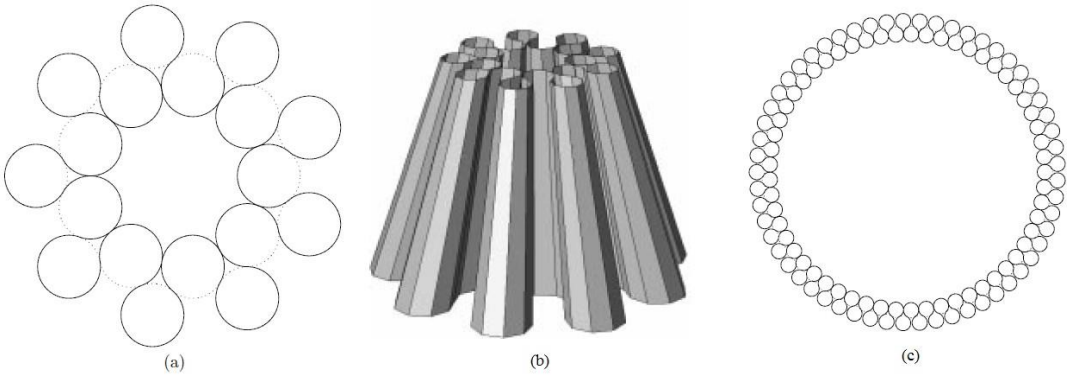

Figure 8 (a) Section using circular shape, (b) corresponding 3D umbrella shape, (c) failure of the umbrella design.

The corresponding results for 6.5 and 16-m diameter mirrors are displayed on Figure 9; the diameter of the 16-m diameter folded mirror is 3.9 m which corresponds to a margin of 15% with respect to the Delta IV rocket fairing inner diameter. In order to determine the free parameters of Eq.1 and Eq.2, the maximal curvature of the section has been minimized according to the three following constraints:

- the number of petals is an integer : $p = \frac{k}{2}, k \in \mathbb{N}$
- the diameter is known and the perimeter is fixed $L = \pi D$
- the stowed membrane must fit into the rocket : $r_0 + \rho \leq R_{Rocket}$

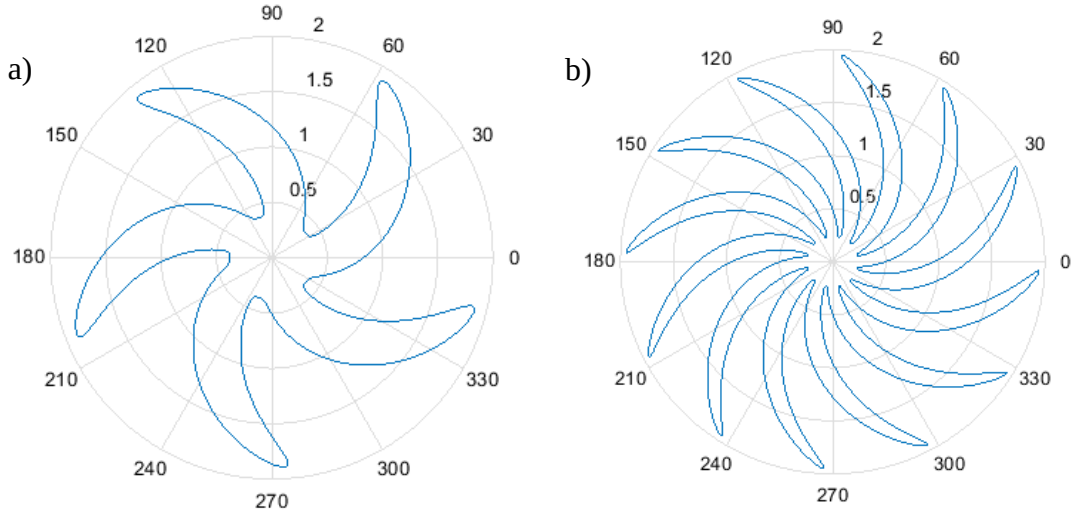

Figure 9 Top section of an umbrella-like folded mirror (a) 6.5-m diameter, (b) 16-m diameter.

First we need to express the derivatives that will be used to compute the circumference and the curvature (see Eqs.3, 4, 5, 6). The circumference is calculated in Eq.7, and the curvature is obtained thanks to Eq.8.

$$\frac{d\theta}{dt} = 1 - 4psin(pt)\cos^3(pt) \tag{3}$$

$$\frac{dr}{dt} = -4p\rho\sin(pt)\cos^3(pt) \tag{4}$$

$$r' = \frac{dr}{d\theta} = \frac{dr}{dt}\frac{dt}{d\theta} \tag{5}$$

$$r'' = \frac{d}{d\theta}\left(\frac{dr}{d\theta}\right) = \frac{4\mathrm{p}^2\rho\cos^2(\mathrm{pt})(1-2\cos(2\mathrm{pt}))}{\left(1-4\mathrm{psin(pt)cos^3(pt)}\right)^3} \tag{6}$$

$$L = \int_{\theta_1}^{\theta_2} \sqrt{\frac{dr}{d\theta}^2 + r(\theta)^2 d\theta} \tag{7}$$

$$\gamma(\theta) = \frac{\mathrm{r}^2 + 2\mathrm{r}'^2 - \mathrm{rr}''}{(\mathrm{r}^2 + \mathrm{r}'^2)^{\frac{3}{2}}} \tag{8}$$

Results for different values of the mirror's diameter are shown on Figure 10 (R_{Rocket} was set equal to 2.1 m but the resulting diameter of the folded membrane can be smaller). The number of petals increases linearly with the diameter of the mirror, while the minimal radius of curvature decreases and can be approximated by a power function of the mirror diameter. Some points of the section, on the outer and inner edges, exhibit very low radii of curvature, leading locally to a greater probability of micro-yield; therefore an analysis of the material's properties is necessary to determine if it can be folded according to those high values of the curvature.

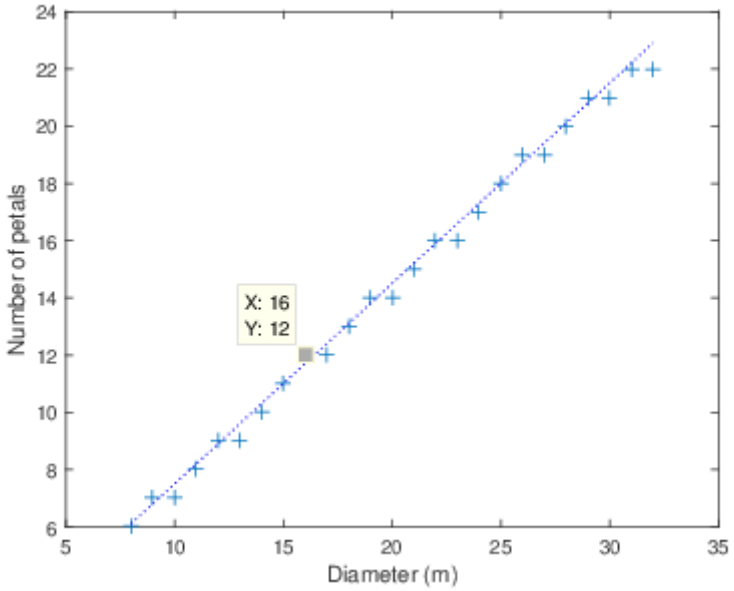

Figure 10 Number of petals as a function of the mirror's diameter.

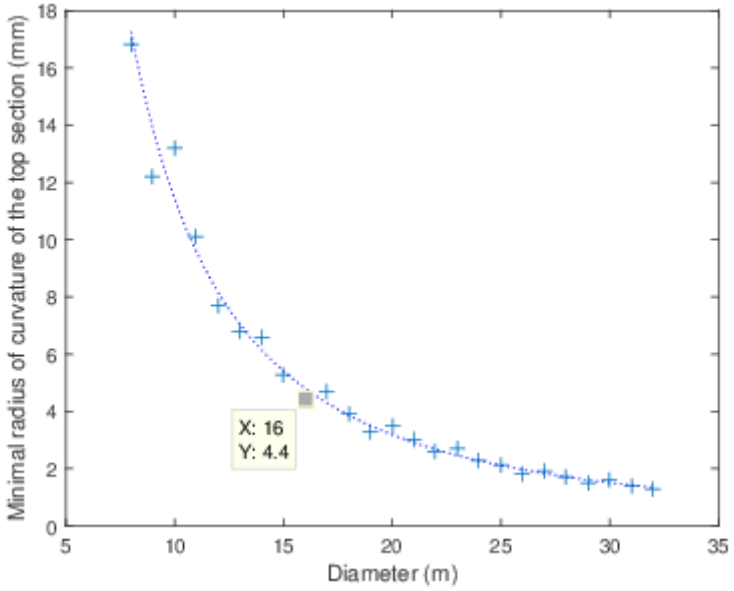

Figure 11 Minimal radius of curvature on the top section for different values of the mirror's diameter.

The corresponding 3D shape has been obtained for a cone: Figure 12 shows the resulting umbrella shape for a 16-m diameter mirror; similar work can be done for a parabola. The final shape has been obtained taking the focal length equal to the diameter: F/D=1. Moreover, the inner hole can be calculated by scaling up the JWST design: $D_{min}/D_{max} = 0.203$ which would give $D_{min} = 3.2$ m for the 16-m diameter mirror. However, for the 3D shape, the minimal radius of curvature is found at the base, not on the top section.

Thus, in order to decrease the risk of micro-yield, one can increase the size of the inner hole, although a portion of the reflective area would be lost. By taking $D_{min}/D_{max} = 0.28$, the inner hole is approximately equal to the maximal size of the secondary mirror, $D_{min} = 4.5$ m. Using this ratio, the collecting surface area represents about 92% of the total surface while, using the ratio of JWST, 96% of the reflecting side would be used. However, the minimal radius of curvature of the lower section of the umbrella is significantly improved, being equal to 1 mm for $D_{min}/D_{max} = 0.28$, against 0.5 mm when $D_{min}/D_{max} = 0.203$.

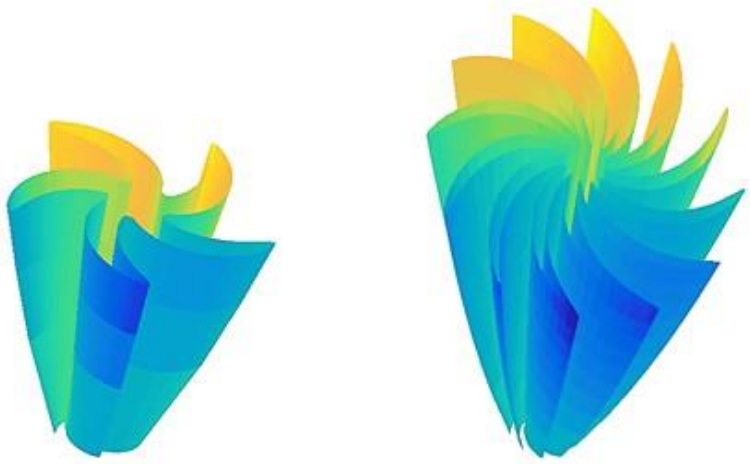

Figure 12 Umbrella-like folded mirror (a) 6.5-m diameter, (b) 16-m diameter (the colors are not meaningful, they are just used for visualization).

5.2.2 Determination of a Condition Before Micro-Yield

There is a minimal radius of curvature allowable before producing micro-yields in the structure; it depends on the materials that are used to make the membrane. The final composition of the membrane is not determined yet but preliminary results have been obtained for materials that are likely to be used. A similar calculation can be done once the composition of the membrane is known. The flexibility of a material, or allowable minimal radius of curvature, can be computed according to the analytic approach of Domber and Peterson [24]. The limit for the minimal allowable radius of curvature, R_F, is achieved when micro-yields appear in the material. Usually, the criterion of the elastic "0.2%" yield stress is chosen, but for optical components even small residual strains must be considered. The calculation of R_F is based on Eq.9.

$$\omega \approx \left(\frac{t}{2R_F}\frac{E}{H}\right)^{\frac{1}{n}}\frac{\widehat{D}^2}{4t} \tag{9}$$

Where ω is the allowable deflection, t is the thickness of the material, E is the Young's modulus of the material, H is the plasticity model constant, n is the strain hardening exponent and $\widehat{D}$ is the length of the surface which is curved. For localized curvature (in the case of the umbrella-like deployment for instance), $\widehat{D}$ can be approximated by $\widehat{D} = 2\pi R_F$ [23]. The main hypothesis behind this formula is that, for very small deformations,

the plastic term in the Ramberg-Osgood model (Eq.11) can be neglected with regards to the elastic term. Eq.9 then leads to Eq.10.

$$R_F \approx \left(\frac{\omega t}{\pi^2} \left(\frac{2H}{tE} \right)^{\frac{1}{n}} \right)^{\frac{n}{2n-1}} \tag{10}$$

The plastic parameter H and the exponent n can be found using the Ramberg-Osgood model for one-dimensional yield:

$$\epsilon = \frac{\sigma}{E} + \left(\frac{\sigma}{H} \right)^{\frac{1}{n}} \tag{11}$$

The strain-stress curves of a material can be approximated by the model represented by Eq.11. For instance, a least-squares approximation, applied to the 23°C strain-stress curve for Kapton® (Figure 13), leads to $n_{Kapton} = 0.238$ and $H_{Kapton} = 0.249\ GPa$ (Figure 15). The same method is applied to Galfenol (Figure 13 and Figure 14). The exponent n takes its value between 0 and 1, and the smaller n is, the more plastic the material is. For aluminum Al 2014-T6, the value for H and n have been found in [24]: H = 0.68 GPa, n = 0.06.

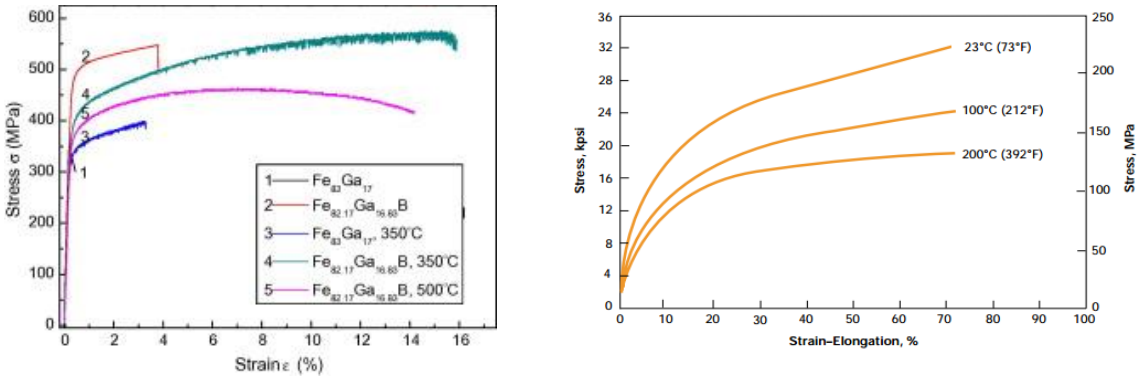

Figure 13 Strain-stress curves for (left) Galfenol [25], and (right) Kapton® (courtesy of Dupont[1] at different temperatures

[1] http://www.dupont.com/content/dam/dupont/products-and-services/membranes-and-films/polyimde-films/documents/DEC-Kapton-summary-of-properties.pdf

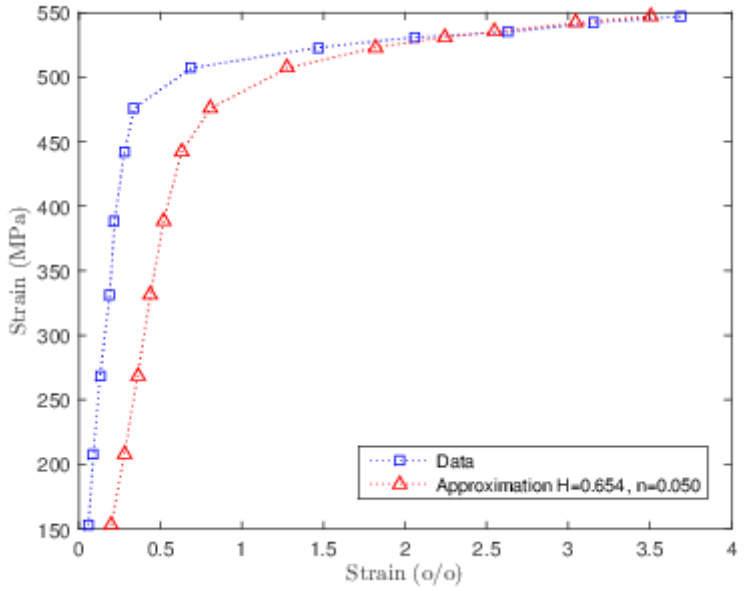

Figure 14 Strain-stress curve for Galfenol ($Fe_{82.17}Ga_{16.83}B$), data and approximation

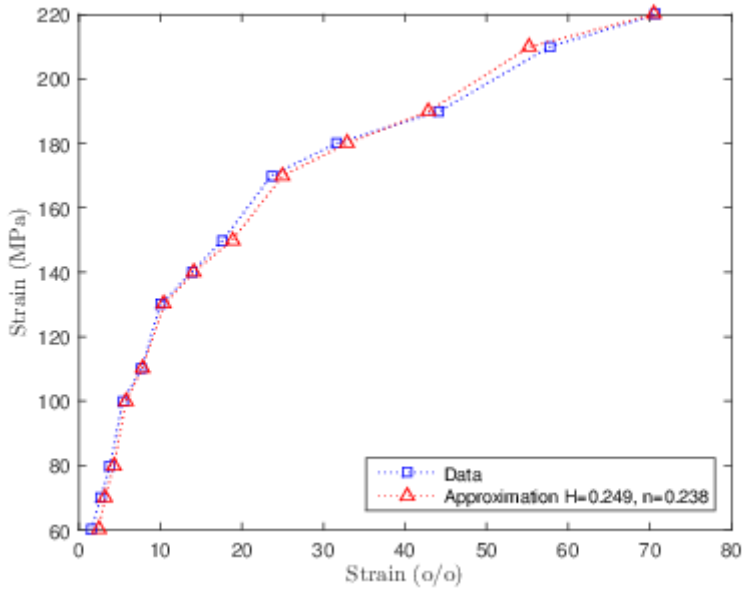

Figure 15 Strain-stress curve for Kapton® (23°C), data and approximation

To compute R_F using Eq.10, a value for the deflection ω must be chosen. Usually, the maximal deflection allowed for a mirror is expressed as a fraction of the shortest operating wavelength of the reflector [23]:

$$\omega_{max} \leq \alpha \lambda_{min}$$

For APERTURE, λ_{min} is taken to be 200 nm (UV). The value for α will be determined during Phase II of the NIAC program, but 1/20 is thought to be a lower limit. Thus, $\omega_{max} \leq 10\ nm$. Nevertheless, APERTURE will get the advantage of post deployment

corrections; hence, it is reasonable to take a higher value for the maximal deflection, say 1 µm. Figure 16 illustrates the impact of ω_{max} and of the thickness on R_F. The results obtained for three types of material are summarized in Table 2. Aluminum, which has a high reflectance for UV, is a candidate for the reflective material, Kapton® may be used as a substrate, and Galfenol is a magnetostrictive material similar to Terfenol-D, but more pliable.

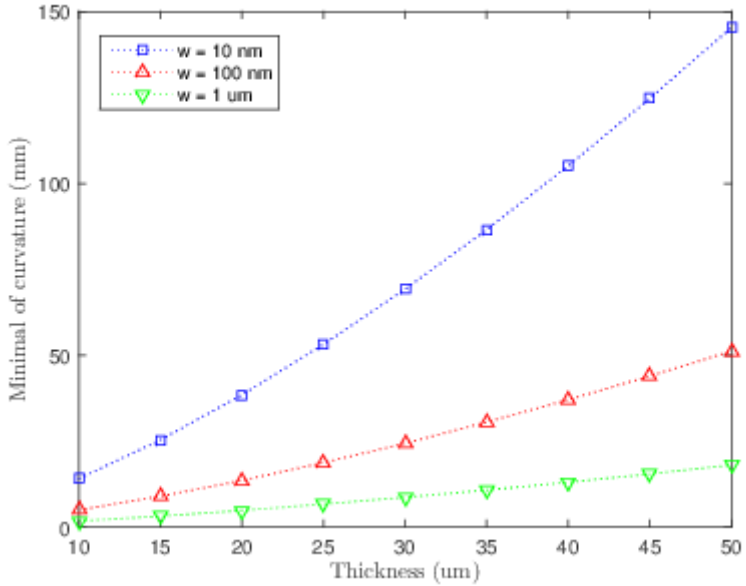

Figure 16 Radius of curvature before micro-yield for Kapton® with different values of the deflection.

Table 2 Pliability, allowable radius of curvature before micro-yield, for different materials and various values of the thickness ($\omega = 1\ \mu m$).

Thickness (μm)	Al 2014-T6 (mm)	Kapton® (mm)	Galfenol (mm)
10	1.2	1.7	1.2
20	2.6	4.8	2.4
25	3.3	6.6	3.1
50	6.9	18	6.3

5.2.3 Deployment Mechanism

Now that the feasibility of stowing the mirror membrane in the Delta IV heavy fairing has been demonstrated, the deployment mechanism needs to be devised. The two main criteria that have been used to characterize the different strategies are the ability to stow the primary mirror into a Delta IV Heavy rocket fairing without damaging the surface, and the possibility of deploying the mirror into space while assuring that the final shape is precise enough to be corrected by applying the magnetic write head on the MSM. Other relevant parameters are the stowed volume efficiency, the stability, and the launch weight. Based on those criteria two types of deployment have been selected to carry out an experimental test campaign in a Phase II. Figure 17 shows a conceptual view of the

flexible primary mirror deployment; a video of the full deployment is accessible online[2].

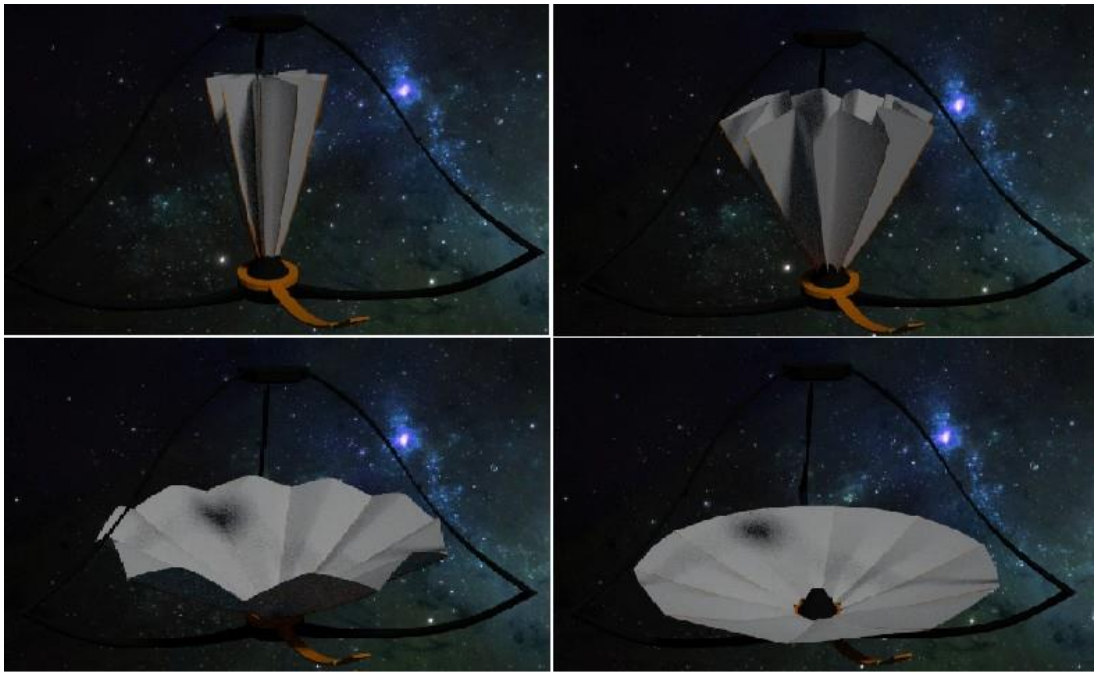

Figure 17 APERTURE deployment (conceptual view), see Figure 1 for the fully deployed telescope

The first design that has been selected is based on the use of a classic composite material combined with an elastic memory composite like TEMBO®. TEMBO® was created by Composite Development Technology (CTD) and was used by Harris Corporation to study the umbrella deployment of a Flexible Precision Reflector (FPR) [26]. The FPR can operate at radio frequencies (40 GHz, wavelength: 7.5 mm) and benefits from a very-low-packaged volume, a potential diameter of 25 m and a very low areal mass density. The reflector is deployed by heating the stiffeners, leading to a gradual, controlled and predictable mechanism (Figure 18).

Figure 18 Flexible precision reflector before and after deployment [26].

An alternative to the umbrella design is the self-deployable shell reflector recently developed by Soykasap et al. [27]. The deployment of a 1.5-m diameter reflector is illustrated on Figure 19. The material used is a Carbon Fiber Reinforced Polymer (CRFP).

[2] Link to video

The size of the reflector is limited by the height of the rocket but a Delta IV heavy fairing would still allow a 17-m diameter primary mirror which is already a notable improvement compared to currently used space telescopes. The deployment of this reflector requires no additional external energy, but the sudden release of stored strain energy can create vibrations in the structure.

Figure 19 Deployment of the self-deployable shell reflector (duration: 1.4 s) [28].

Table 3 summarizes the main characteristics of the prototypes that have been manufactured according to the two designs described above. The RMS error values can be compared to the magnitude of the maximal deflection that one can obtain using MSM discussed in 5.1.4. The CRFP may prove too stiff, but the FRP has quite a low Young's modulus, measured in tens of kPa [29].

Table 3 Characteristics of the two selected deployment designs.

Design	Diameter	Thickness	Material	RMS error
Flexible Precision Reflector (FPR) [26]	0.9 m	152 μm	TEMBO®, elastic memory composite	330 μm
Self-deployable flexible shell [27]	1.5 m	220-880 μm	CRFP, plain weave	420 μm

5.3 Operation and Characteristics of the Post Deployment Shape Correcting System

In order to avoid the risks of having a fixed wire attached to a moving component, the magnetic write head will be wireless and will be powered by a battery which will be recharged on a charging station. The initial design of APERTURE, illustrated on Figure 1 (see also the animation referenced in 1 and 5.2.3 includes only one magnetic write head moving on a single arm. However, this design will likely be modified given the size of the 16-m primary mirror; indeed, if the time during which the MSM holds its shape is shorter than the time needed to correct the shape using a single magnetic write head, then APERTURE would not be feasible. Thus, it is necessary to determine how many magnets are required to make post deployment corrections fast enough. Other parameters like the size of the magnet's battery or the percentage of the spacecraft's main battery which is allocated to the magnetic write head can influence the duration of the correction process.

To carry out this analysis, a worst-case scenario is chosen, assuming that the entire back of the mirror needs to be corrected by the magnetic write head; the duration of the

correction process is T_{tot}. A first estimation of T_{tot} can be obtained using $T_{tot} \approx S_{tot}/S_{mag} \times T_{mag}$, where S_{tot} is the total surface area of the mirror, S_{mag} is the surface of the magnet and T_{mag} is the time spent for correcting S_{mag}. However, this calculation is not realistic enough, it does not take into account several phenomenon, such as the fact that the magnet needs time to be recharged, or the limitation of the number of battery cycles per day. Hence, a more comprehensive calculation is needed to have a better estimation of T_{tot}. For comparison purposes, the baseline used for the calculation is that of JWST but with a diameter of 16 m. The influence of different variables is studied by varying one parameter at a time. The list of the parameters that are used, along with their nominal value, can be found in Table 4.

5.3.1 Baseline Values of the Parameters

This section justifies and clarifies the baseline values that have been chosen for the different variables. For the solar arrays, the JWST will have approximately 26 m² of solar panels[3] but we choose to use an optimistic version of the JWST with photovoltaic panels of 31 m². To compute the input power of the solar arrays we use two methods. First we use radiation theory assuming that APERTURE, like JWST, is located at the Sun-Earth Lagrangian point L2 on a Lissajous orbit with a semi-major axis of 800,000 km [30]. This Lissajous orbit is approximated by a circular orbit with a radius equal to its semi-major axis. The Sun is considered to be a black body with a temperature of $T_{Sun} = 5778\ K$. The total power emitted by the Sun is computed according to Eq.12. The solid angle Ω under which the telescope sees the Sun is computed from to Eq.13, where h is the radius of the orbit and d is the distance between the Sun and L2, $d \approx 1.515 \times 10^8\ km$. Then the power received by the solar panels is equal to the total power emitted by the Sun times $\Omega/4\pi$, the percentage received by the telescope (Eq.15).

$$P_{Sun,tot} = 4\pi R_{Sun}^2 \sigma T_{Sun}^4 \tag{12}$$

$$\Omega = \frac{A_{Arrays}}{d^2 + h^2} \tag{13}$$

$$P_{received} = \frac{\Omega}{4\pi} P_{Sun,tot} \tag{14}$$

$$= \sigma T_{Sun}^4 A_{Arrays} \frac{R_{Sun}^2}{d^2 + h^2} \tag{15}$$

The photovoltaic cells that are used are GaAs cells with an efficiency of 18% [31]. The result using this method is $P_{received} = 7431.44$ W. In order to confirm this result, we compare it to the polynomials method used in [32] and illustrated on Figure 20, with $P_0 = 1358$ W/m². We found $P_{received} = 7442.82$ W, which is very close to the value we computed.

[3] http://jwst.nasa.gov/bus.html

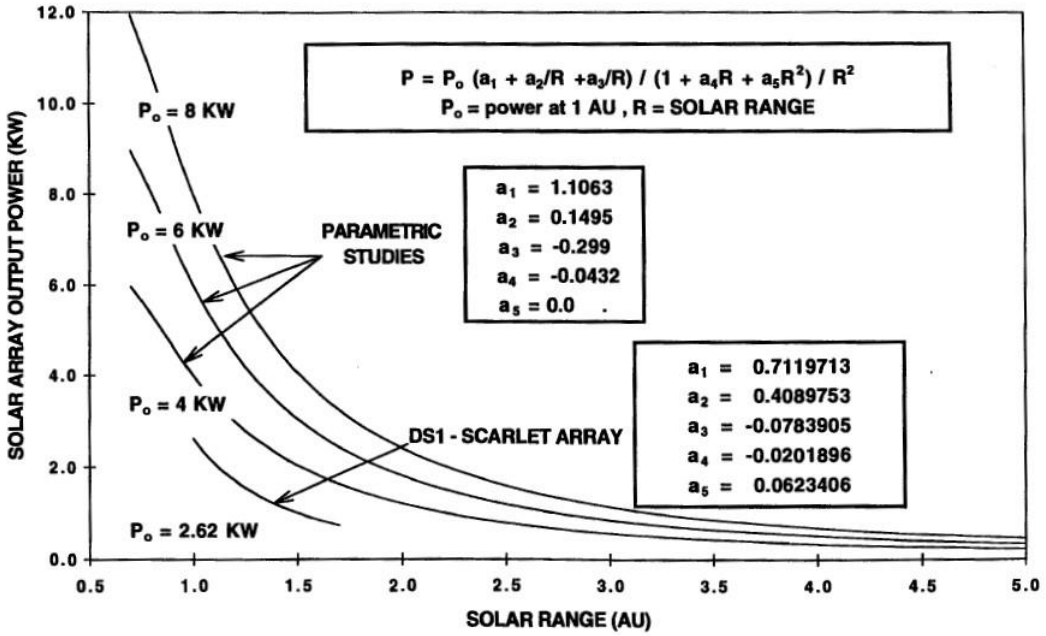

Figure 20 Solar array output power versus solar range using polynomials method [32].

JWST will use a 37 Ah NiH2 battery and the nominal mission operating voltage is predicted to be between 30 and 32 V [30]. Hence, we take an average voltage of 31 V to calculate the size of the battery which is $37 \times 31 \times 3600 \approx 4 \times 10^6$J. The efficiency of the battery is 85%; note that this efficiency should decrease during the mission but it is taken constant to simplify the calculation. The depth of discharge (DOD) of the battery is 35%, like JWST [30]. This allows us to calculate the number of cycles per day using the method described on page 404 in [31] (see 5.3.4). The nominal value of the mission lifetime is set equal to the maximal lifetime of JWST, which is 10 years [30]. Using 10 cycles per day we find DOD = 39% which is very close to the value indicated for JWST. In order to estimate the percentage of the battery that will be allocated to charge the magnet in the APERTURE concept, we need to determine how much energy is required for other subsystems like the communication system. According to [33], JWST requires a communication time of 8 hours per day. We were not able to find exact specifications of JWST communication system but considering the DOD, the number of cycles per day and the duration of communication, we estimate the percentage of the battery that is allocated to the communication subsystem, is ≈ 4.87%. Now, based on the work done at Northwestern University about magnetic write heads (section 5.1) we know that the magnetic write head requires a few Watts to work, hence we set the power required by the magnetic write head equal to 5 W. This value will need to be refined for future work and will be precisely measured during Phase II. Assuming that the magnetic write head is used all the time, we calculate that we can allocate about 1.72% to charge the magnetic write head. This leaves 93.41% for the other subsystems like the attitude determination and controls or the scientific instruments. This of course is a very simplified configuration, but it will give us an estimate of the time required to correct the mirror. For the magnetic write head battery we assume a baseline size of 2×10^5 J which corresponds approximately to a laptop battery. Using [31] we compute a DOD of about 49% for the given mission lifetime and this corresponds to a baseline value of about 4 cycles per day for the magnet battery. Finally, for the baseline case we assume we only have one magnet and that it covers an area of about 1 cm² during a time of 3 s. The last

two values give an order of magnitude of what we expect those parameters to be, but they will be accurately quantified during Phase II; they depend on cost and manufacturing issues along with the duration of the shape assessment process and other variables.

5.3.2 Diameter of the Primary Mirror

As expected, T_{tot} increases with the diameter of the mirror; more precisely it is a linear function of the diameter squared (Figure 21). This parameter has a large impact on the duration of the figure correction process. It is not a free parameter of the design given that the baseline for the APERTURE concept is a 16-m diameter primary mirror, but this analysis shows that the size of the telescope is not only limited by the rocket fairing but also by the time required to correct its shape.

5.3.3 Mission Lifetime

The mission lifetime drives the depth of discharge (DOD) of the battery of the spacecraft and of the magnet; when the mission lifetime increases, the allowed DOD decreases according to Eq.16 which we derived from Figure 22 found in [31]:

$$DOD(\%) = -12.1602 \times Ln(NbCycles) + 166.9983 \qquad (16)$$

where $NbCycles$ is the total number of cycles of the battery during the mission. Eq.16 corresponds to Nickel Cadmium batteries. To study the impact of this variable, the number of cycles per day has been taken constant. As shown on Figure 23, T_{tot} increases with the mission lifetime but, in order to maximize the mission goals, we preferred to keep the mission lifetime fixed, equal to JWST maximal lifetime, that is to say 10 years.

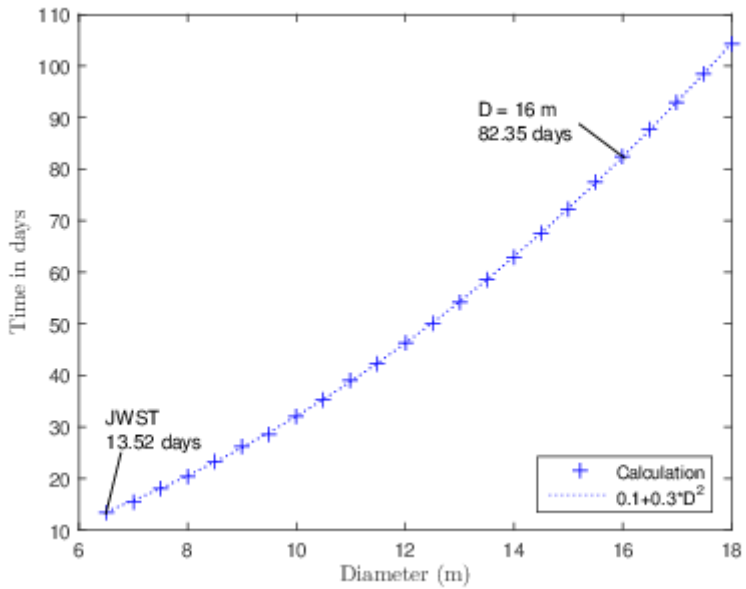

Figure 21 Time spent to correct the entire membrane as a function of the mirror's diameter.

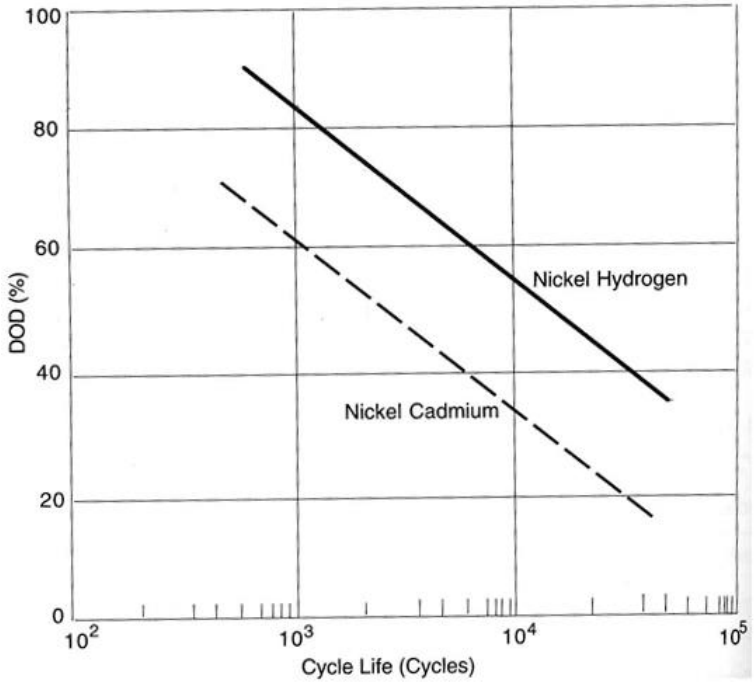

Figure 22 Depth-of-discharge versus cycle life for secondary batteries [31].

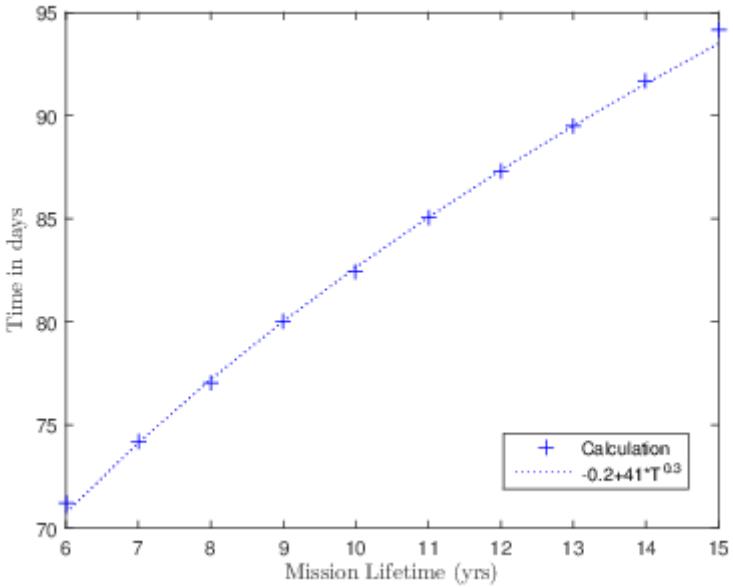

Figure 23 Time spent to correct the entire membrane as a function of the mission lifetime.

5.3.4 Number of Cycles of the Magnet Battery

To study the impact of the number of daily cycles of the magnet battery, we take the mission lifetime equal to its baseline value, but the DOD can vary. As it is illustrated on Figure 24, this parameter does not have a huge impact on T_{tot} since it stays between 82.28 and 82.48 days over the entire range. Hence, this parameter is not crucial and does not drive T_{tot}.

5.3.5 Number of Cycles of the Main Battery

Similarly, we take the mission lifetime equal to its baseline value but the DOD can vary. As one can see on Figure 25, T_{tot} decreases with the number of cycles of the main battery until a threshold value, ≈ 20 cycles/day, at which T_{tot}become constant. This change of T_{tot}behavior can be explained by the limited size and performance of the magnet battery: allowing the battery to recharge a large number of times per day is not necessary; there is a point at which the performance of the magnet battery becomes the limiting factor.

5.3.6 Percentage of the Main Battery Allocated to Charge the Magnet

Figure 26 shows that T_{tot} decreases when a larger part of the main battery is allocated to charge the magnet, until a certain value, ≈ 2.8%, after which T_{tot} stays constant. This large change of T_{tot} behavior can be explained by the limited size of the magnet battery. Hence, it is not necessary to take a percentage greater than 3% for the values of the parameters that are used to make this calculation.

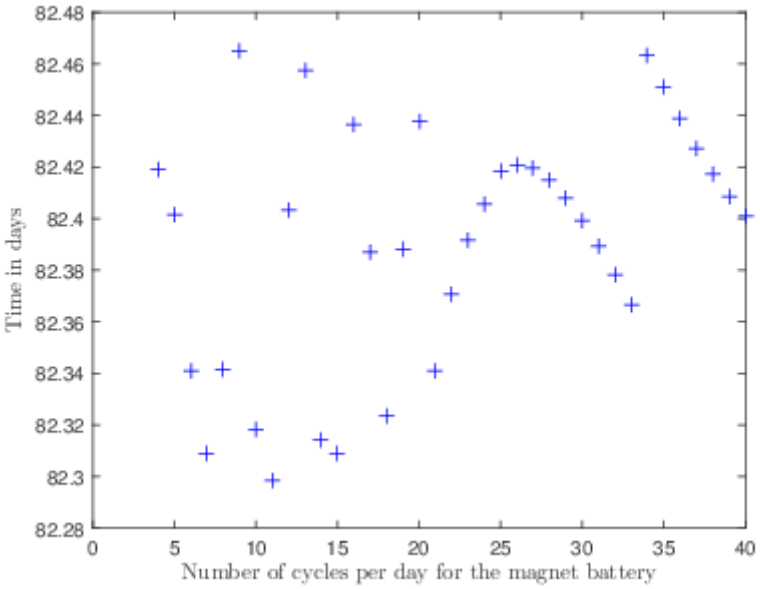

Figure 24 Time spent to correct the entire membrane as a function of the number of daily cycles of the magnet battery.

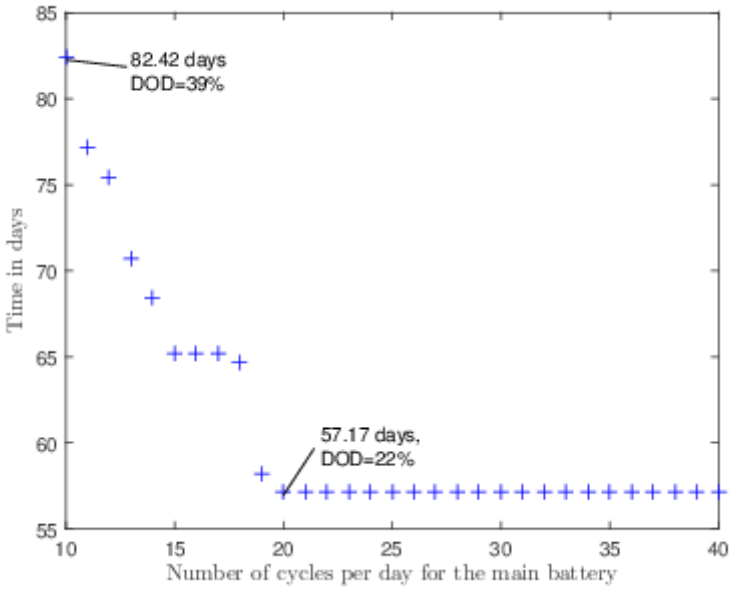

Figure 25 Time spent to correct the entire membrane as a function of the number of daily cycles of the main battery.

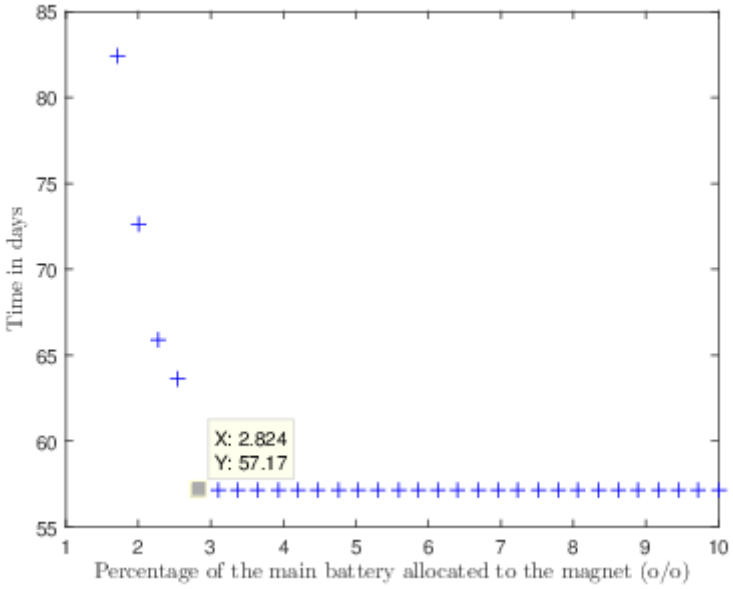

Figure 26 Time spent to correct the entire membrane as a function of the percentage of the main battery allocated to the magnet.

5.3.7 Size of the Magnet Battery

The size of the magnet battery has a huge impact on the time required to correct the shape of the mirror, however, Figure 27 displays a horizontal asymptote. Hence, it is not really worth it to take a battery that is larger than the maximal value displayed on Figure 27, which has the same characteristics as a laptop battery.

5.3.8 Size of the Solar Panels

The size of the solar arrays has a very small impact on T_{tot} as one can see in Figure 28. This variable only changes the power used to charge the spacecraft main battery, hence the time it takes to recharge this main battery. It can be compared to the size of the solar panels for Hubble, which has two panels[4] of 2.45×7.56 m, and to Rosetta[5], which has 64 m². Since it is not a driving factor, the area of the solar panels can be taken equal to those of JWST.

5.3.9 Surface of the Magnet

As illustrated on Figure 29 and as expected, the time necessary to correct the shape of the mirror decreases with the surface of the magnet, but the larger the magnet is, the closer to zero the slope gets. Note that this parameter is not totally free, it both depends on the difficulties in manufacturing large magnetic write heads, and is limited by the minimal accuracy than one needs to control the parabolic shape. Hence, the value chosen for the preliminary design is likely to be modified but it is a credible estimation of the final value.

5.3.10 Time Allocated to Each Location

T_{tot} increases linearly with the time spent to correct each point or "pixel" of the mirror, with a slope of 28 days/s. Similarly to the size of the magnetic write head, this variable cannot be chosen freely. It depends on the reaction time of the magnetic smart material, on the shape assessment duration, and on the convergence speed of the corrections.

5.3.11 Number of Magnets

The number of magnets has a high impact on the time required to correct the primary. However, the curve displays a horizontal aymptote (see Figure 31), hence, after a certain value, the benefits of adding more magnets, which are a diminution of both T_{tot} and the failure risk thanks to redundancy, do not compensate the consequent drawbacks, which are the increased mass and complexity. For the preliminary design, 8 magnetic write heads are chosen.

[4] www.spacetelescope.org/about/general/fact_sheet/
[5] www.esa.int/Our_Activities/Space_Science/Rosetta/Frequently_asked_questions

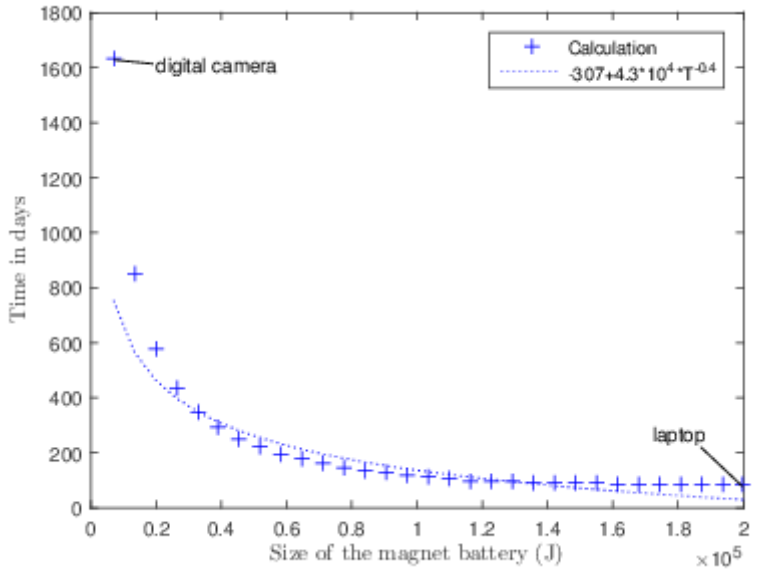

Figure 27 Time spent to correct the entire membrane as a function of the size of the magnet battery.

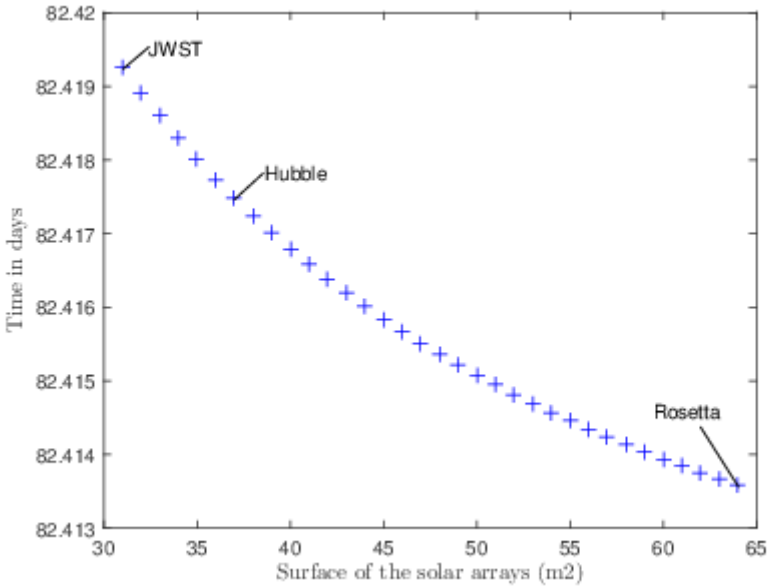

Figure 28 Time spent to correct the entire membrane as a function of the size of the solar panels.

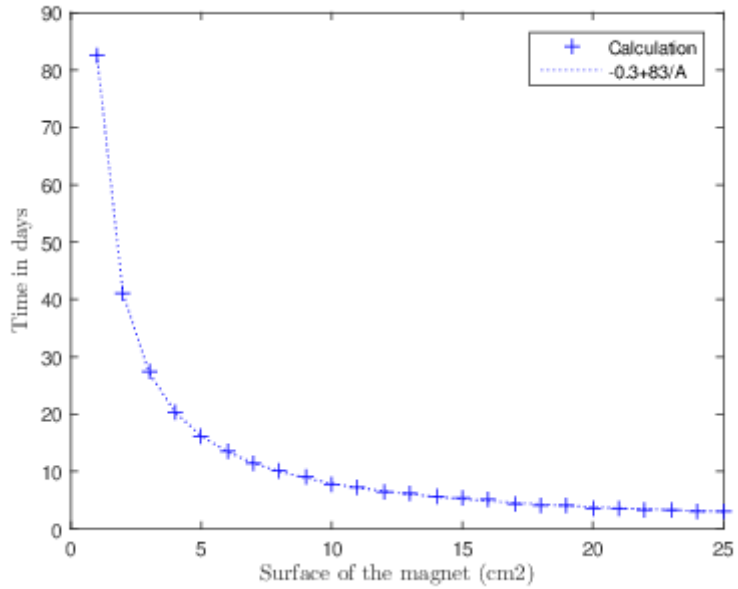

Figure 29 Time spent to correct the entire membrane as a function of the surface corrected by the magnet.

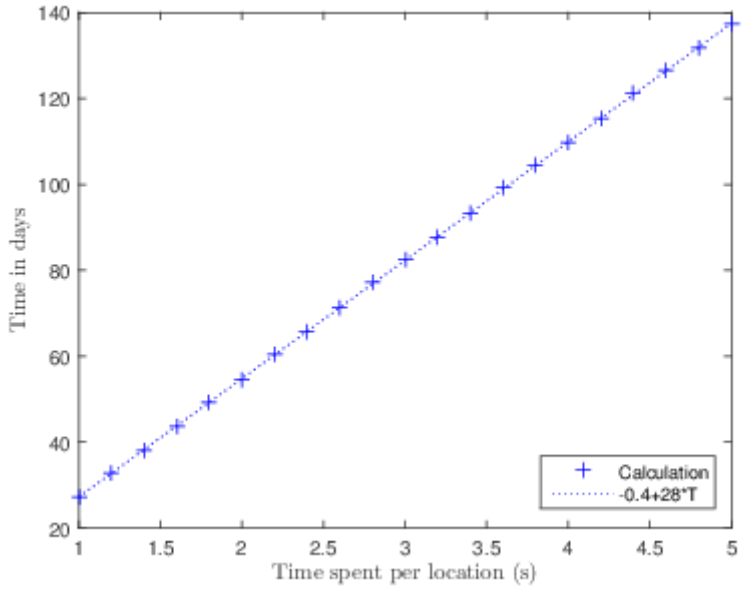

Figure 30 Time spent to correct the entire membrane as a function of the time allocated to each points that needs to be corrected.

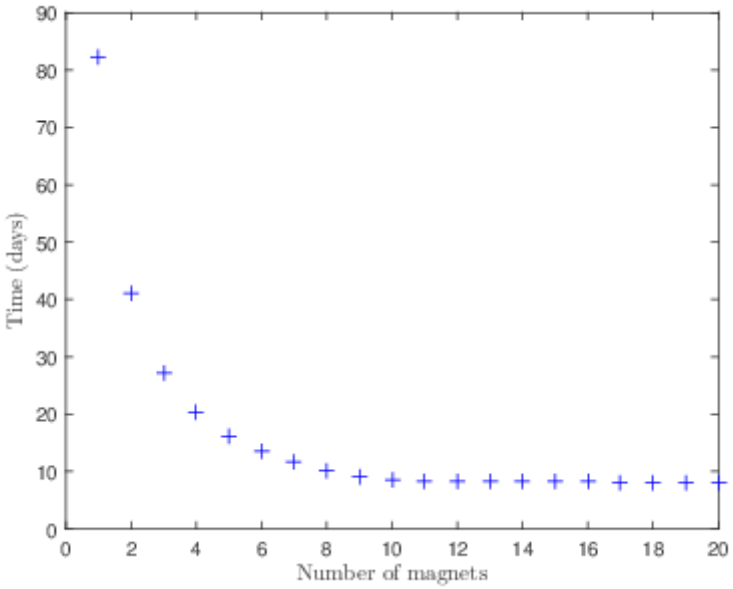

Figure 31 Time spent to correct the entire membrane as a function of the number of magnets.

5.3.12 Summary

Table 4 shows a summary of the study described above. The influence of each variable can also be quantified by the percentage of impact which is taken equal to $\Delta T \frac{\Delta V}{V}$, where V is the baseline value given to the parameter when another variable is studied, ΔV gives the range of values taken by the parameter when its impact is computed, ΔT is the difference between the maximal and minimal T_{tot}. The result is shown in Figure 32. As one can see, using this definition of the percentage of impact, the most significant parameter is the size of the magnet battery. Thus, the time required to correct the shape of the primary in this worst-case scenario can be greatly improved if the design and manufacturing constraints allow for larger magnetic write head batteries. In order to compare the impact of the other studied variables, Figure 33 has been obtained by removing the data corresponding to the magnet's battery. Once setting the diameter of the mirror equal to a certain value, one can use the most significant parameters, which are the size of the magnet's battery, the time allocated to each point, the mission lifetime, the number of daily cycles for the main battery, the number of magnets, and the surface of the magnet, in order to create an optimal design and meet the requirement in terms of time spent to correct the shape of the membrane. This analysis enabled us to identify the most important variables that we will need to take into account to create the optimal design for APERTURE.

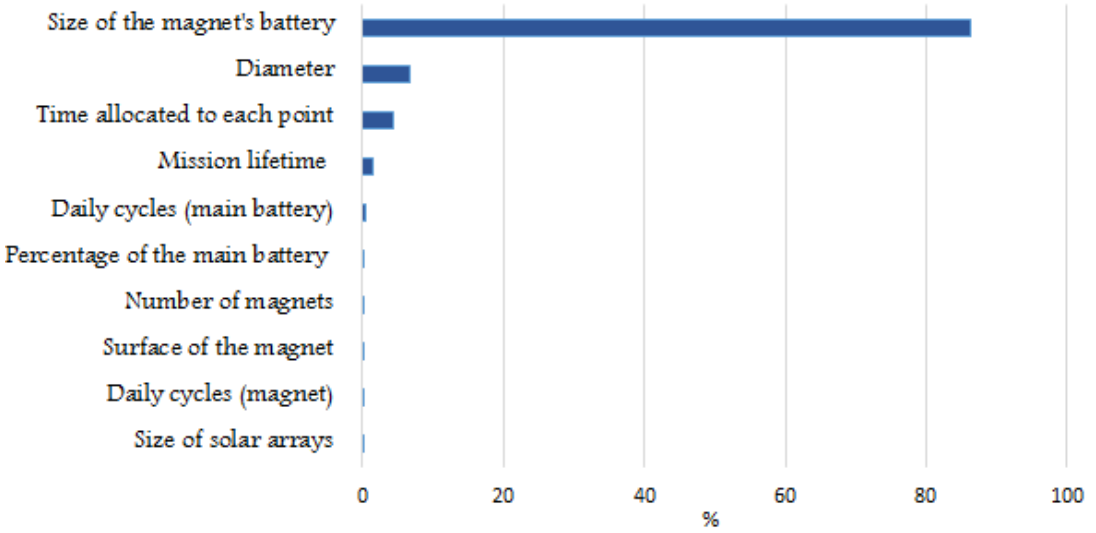

Figure 32 Quantification of the impact of different parameters on the time needed to correct the entire mirror (with all parameters included).

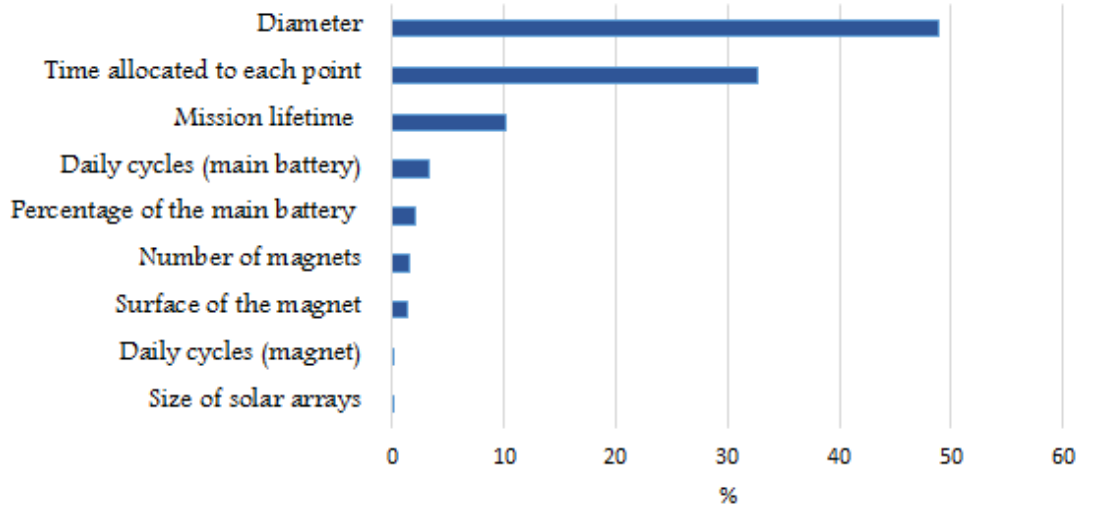

Figure 33 Quantification of the impact of different parameters on the time needed to correct the entire mirror (with all parameters except for the size of the magnet battery).

Table 4 Summary of the impact of different parameters over the time required to correct the mirror.

Parameter	Range	Nominal Value	Constraints	Impact	Horizontal Asymptote	Preliminary design
Diameter	6.25 – 18 m	16 m	Rocket fairing	High	No	16 m
Mission lifetime	6 – 15 yrs	10 yrs	Mission goals, Battery perfomances	Moderate	No	10 yrs
Daily cycles (magnet)	4 – 40 cycles/day	4 cycles/day	Battery Performances	Very Low	No	11 cycles/day
Daily cycles (main battery)	10 – 40 cycles/day	10 cycles/day	Battery Performances	Moderate	Yes	20 cycles/day
Percentage of the main battery used to charge the magnet battery	1.72 – 10 %	1.72 %	Other subsystems requirements (communication, instruments…)	Moderate	Yes	3%
Size of the magnet's battery	7.E3 J (digital camera) – 2.E5 (laptop) J	2.E5 J	Mass requirement, Performances of the arm holding the magnet	Very High	Yes	2.E5 J
Size of solar arrays	31 m^2 (JWST) – 37 m^2 (Hubble) – 64 (Rosetta) m^2	31 m^2	Rocket Performances (mass) and Dimensions	Very Low	Yes for large values	31 m2
Surface of the magnet	1 – 25 cm^2	1 cm^2	Manufacturing Limitations	High	Yes	2 cm2
Duration to treat each location	1 – 5 s	3 s	Magnetostriction properties, shape assessment duration	High	No	3 s
Number of magnets	1–20	1	Mass requirement	High	Yes	8 magnets
					Total time	3.68 days

5.4 Preliminary APERTURE Design

5.4.1 Magnetic Smart Material and Substrate

As noted in section 5.1, there are a wide range of MSMs available. For simplicity we choose the strongest one, Terfenol-D, but Phase II funding would allow us to explore the approach of using a material that has both strong enough magnetostriction and high remanence, such as Vanadium-Permadur. Based on initial deflection studies on glass with an approximate 0.1 T field and a 4 μm Terenol-D film, we will base line a 4 μm Terenol-D film, and < 1 μm NiCo film or FeCo film to hold in the magnetic field. The substrate could be as thin as 5 μm made up of a polyimide such as Kapton® or CP-1. An alternative approach would be to use some shape memory composite whose front surface could be shiny electro-formed material such as Ni which is known to have a deployed shape good enough for the microwave regime [34].

5.4.2 Magnetic Write Head

The very tentative design would be a horseshoe geometry of soft magnetic material such as iron with a gap separation of 3 mm to 1 cm or even larger. With larger spacing, a stronger current and more windings would be needed, but conversely, the larger (within reason, i.e. no more than ≈10 cm) the size of the ``pixels" of the mirror that can be corrected, the better. It is true because a larger pixel size means fewer total pixels that will need correction. If the power requirement becomes too great, the fall back is to use permanent magnets whose gap strength can be controlled mechanically. We give an example of each type of design in Figure 34.

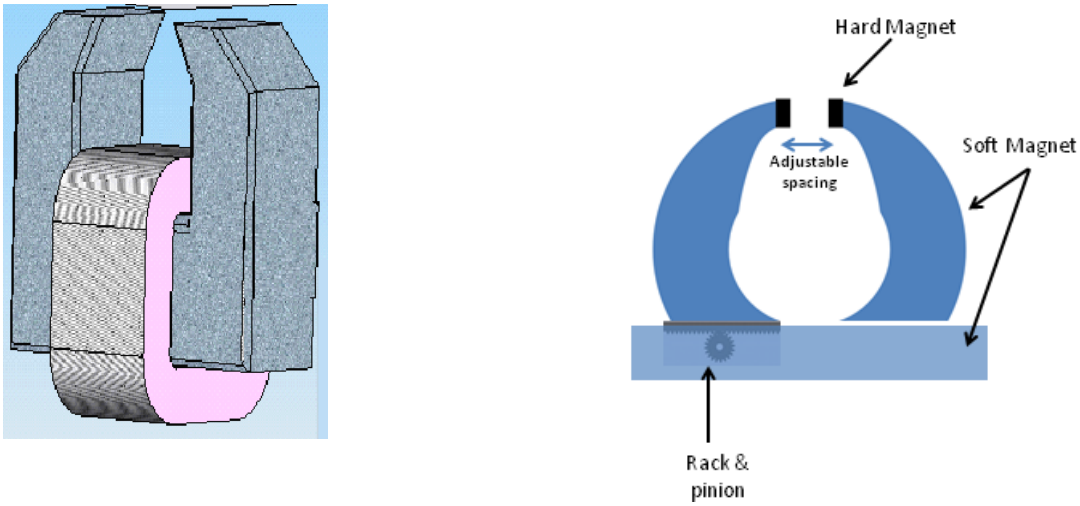

Figure 34 In both cases the magnets have been designed so that the magnetic field runs primarily parallel to the surface. Left: Simplified drawing of an electromagnet provided by Dr. C. Joshi of Altranex Corp. Ontario, Canada. Right: Schematic of a permanent magnet design whose effective magnetic field strength can be adjusted, courtesy of Drs. C. S. Arnold and D. Pappas of NIST Boulder, Colorado, USA.

5.4.3 Operation and Characteristics of the Post Deployment Shape Correcting System

The estimation of the time required to correct an entire 16-m mirror, with a single magnetic write head, and using the baseline values of Table 4, is about 82 days, but this number can be reduced by adding magnetic write heads and changing the other significant variables. An example of a modified design is proposed in Table 5 and corresponds to a total time of only 3.68 days. When the shape assessment, feedback process and parameters of the magnetic write heads are known in details, the various design parameters used in section 5.3 can be computed to obtain an optimal and feasible design for operation management.

Table 5 Alternative design, reduced total time

Diameter	16 m
Mission lifetime	10 yrs
Daily cycles (magnet)	11 cycles/day
Daily cycles (main battery)	20 cycles/day
Percentage of the main battery used to charge the magnet battery	3%
Size of the magnet's battery	2×10^5 J
Size of the solar panels	31 m^2
Surface of the magnet	2 cm^2
Time allocated to each point	3 s
Number of magnets	8
Total time	3.68 days

5.4.4 Stowed Configuration and Deployment Mechanism

The primary mirror membrane can be stowed in a Delta IV Heavy rocket using the umbrella design introduced in section 5.2.1. The preliminary design assumes a focal length equal to the diameter of the primary mirror. The secondary mirror and the inner hole of the primary mirror have a diameter of 4.5 m, which corresponds to the utilization of 92% of the available light-collecting surface area. The height of the stowed membrane is about 8 m while its diameter is 3.9 m. This design exhibits very low local radii of curvature, the minimum being 1 mm. Hence, to avoid any risk of micro-yield, if aluminum is used as the reflective layer, Kapton® as the substrate and Galfenol as the magnetostrictive material, they have to be less than 8 μm, 7 μm and 9 μm respectively (see section 5.2.2). This may not be the final composition of the membrane but the same method can be applied to other materials once they are selected. The deployment of the umbrella membrane will be based on the flexible reflector presented in section 5.2.3 which uses a memory composite material, leading to a slow and controlled deployment. An alternative design is the self-deployable shell reflector (see section 5.2.3) which can be used for reflectors up to 17-m given the height of the Delta IV Heavy rocket fairing, while the umbrella design could be scaled-up. In all cases, the RMS

figure accuracy will need to be reduced from its deployed value in order to be effective for the UV-Vis wavelength range.

5.4.5 Post Deployment Figure Assessment and Feedback

Two designs have been selected from a literature survey. The first design is that being used for JWST [35] which involves determining where a reference star is imaged from each segment in an out of focus image. Then, each segment is adjusted via a tip-tilt and push-pull until each star image is at its proper location. In the second approach, a standard Shack-Hartmann test is used to adjust the figure [36].

5.5 Concept Verification Testing

Several tests are proposed to validate the main concepts of the APERTURE system including MSM mirror reflection and deployment tests. The Shack-Hartmann wavefront sensor test is an optical method for determining the wavefront shape of a parabolic mirror. Shack-Hartmann sensors provide accurate wavefront shape feedback via measurement of the localized slope of the wavefront error. This measurement is performed using a lenslet array to split the incoming wavefront into an array of smaller beams. Each beam is focused onto a CMOS camera placed on the focal plane of the lenslet array [37]. Each lenslet creates a spot along the optical axis which can be used to calculate the local wavefront tilt across each lens. A non-distorted wavefront creates a regularly spaced grid of spots, while a distorted wavefront causes some lenslets to displace their corresponding spots and create an irregular grid. Therefore, the whole wavefront shape can be determined from the grid spots provided by the lenslet array. Figure 35 illustrates the figure when the shape is correct (A) and when it needs correction (B).

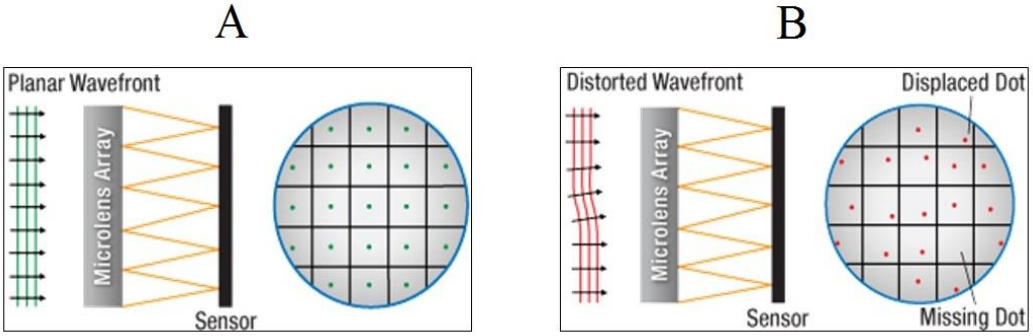

Figure 35 (A) Image of a regularly spaced grid. (B) Image of a grid from a distorted wavefront [37].

A Shack-Hartmann test implements a simple setup for the testing of optical lenses and mirrors. It consists of a point source, Shack-Hartmann wavefront sensor, laser collimating lens, beam reducer, beam splitter, illuminating lens, and a reference lens. Table 6 identifies these components along with their characteristics. Figure 36 shows the setup geometry of the test components for the testing of the reference lens, as determined by the National Institute of Standards and Technology [38].

For the purposes of validating an MSM reflective mirror, the test will be performed vertically instead of the traditional horizontal setups. This allows the gravity to aid the MSM membrane to maintain its curved shape. The location of the components relative to each other is a function of the focal length of the mirror. A laser diode in the visual spectrum will be the point source for this experiment. The illuminating lens is sized to guarantee both the reflected light of the mirror and the laser diode cover their respective targets. This size is a simple function of the focal length as well as the wavefront sensor aperture size. S_0 and S_i represent the distances between the Beam Reducer and Illuminating Lens and between the Illuminating Lens and the Object Under Test, respectively. They were found to be 27.5 cm and 2.75 cm using equations (5) and (6).

$$S_o = f_1 + f_t \tag{17}$$

$$S_i = \frac{f_1^2 + f_t f_1}{f_t} \tag{18}$$

Table 6 Shack-Hartmann Test Components

Component	Manufacturer and Part Number	Characteristics
Wavefront sensor	Thorlabs WFS300-14AR	300 μm Pitch, AR Coated: 400-900 nm
Beam Reducer	Thorlabs GBE03-A	3X Expander,AR Coated: 400-650 nm
Beam Splitter	Thorlabs BS025 - 10:90 (R:T)	Non-Polarizing Cube 400-700 nm, 1"
Illuminating lens	Thorlabs LA1560-D	12.7 mm Diameter, 25 mm Focal Length
Reference Lens	Newport Concave Lens	50.8 mm Mirror, 250mm EFL

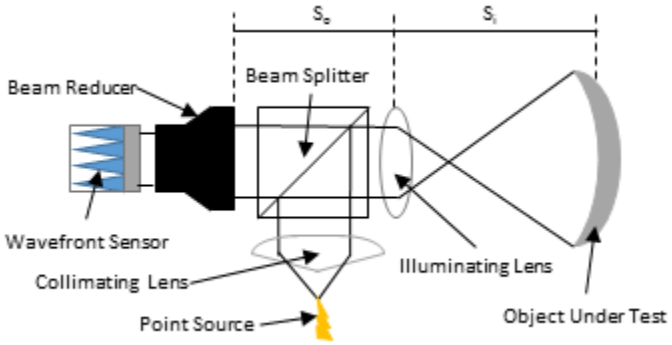

Figure 36 Test Geometry for Shack-Hartmann

As mentioned above, a deployment verification test will need to be performed. The purpose of this test is to show that the aforementioned deployment method will unfurl the membrane without it ripping or catching. A scale model test could be performed in one of two ways, using the deployment mechanisms selected in section 5.2.3. Both ways would use an analog material to the MSM membrane to reduce test cost. The first method would be a powered test using powered actuators. The other option is an empowered test using springs. The exact details of this test will be worked out at the initial portion of Phase II.

6 Work Plan for Phase I

6.1 Tall Poles for Phase II

Even though no showstoppers have been found during Phase I, the team has identified possible obstacles and questions that remain for the APERTURE Concept. In order of precedence:

1. Can we get any membrane-like material to deform in a controlled manner and have the shape remain for days to weeks, minimum?
2. Can the two selected deployment mechanism produce a near net shape to about 300-400 μm that will have such a low in-plane stress that further correction via magnetostriction is possible?
3. Can the deployed membrane be such that any required corrections are on length scales greater than 1 cm, as correcting mm length scale errors would be extremely challenging?
4. Is a closed-loop controller possible for in orbit figure assessment and correction?
5. Are the disparities in the materials' Coefficients of Thermal Expansion (CTE) critical for the shape correction process? Is thermal control necessary, in particular because of shape memory composite?
6. Can pieces of membrane be stitched together as it would be technically challenging to coat a monolithic 16 m (or larger) diameter mirror?
7. Can the position of the magnet be accurately determined and controlled, both in distance from the substrate and in radius and azimuth relative to the optical axis?
8. Is a secondary deformable mirror a credible path given that, the smaller the deformable mirror, the smaller the resulting field of view?
9. Instead of being placed at the L2 point, can APERTURE be used in GEO?

Question 1 was partially answered during Phase 1 but it needs more in-depth investigation, especially about the in-plane stretch. The membrane boundary may need active control which could also counteract the elastomer creep produced under UV exposure. This first topic will be investigated through Tasks 1 and 2, which will also address item 4. Questions 2 and 3 are very challenging since deployed membranes tend to have systematic-type errors and low spatial frequency errors that are hard to eliminate. Those issues will be tackled with Task 3. Question 5 about thermal control has not been addressed during Phase I, and time may not permit to investigate

this topic but the team will complete the different tasks of Phase II keeping in mind that thermal control may be critical. For instance, while choosing the materials in Task 1.1, the CTEs will be taken into account. Temperature can be controlled thanks to a sun shield, a material combination that offers minimal mechanical response under thermal gradients, or by an active system. Some of the other questions may be addressed in Task 5 if time permits.

6.2 Task Breakdown

During Phase I, no show stoppers were found, albeit we are far from a final working proof of concept. Thus, continued study into the material selection for the MSM and substrate, deployment design and implementation, and magnetic write head design is required to confirm the viability of APERTURE. A Phase II effort will perform proof of concept experiments for the critical items of deployment and surface correction. Several 5×5 cm or 10×10 cm flat samples with different substrates and MSM coatings will be fabricated for testing plane rectification. The exact size will depend on the details of the coating process(es) used, .e.g. sputtering on 5×5 cm flat sample is straight forward as is electroplating 10×10 cm pieces. Also, several stowed prototypes will be created to explore deployment strategies. Along with the experiments, detailed numerical modeling and simulations will be performed.

The *Herschel* telescope worked in the range about 50-700 μm and had a diameter of 3.6 m [39]. Thus a first step in our development would be to achieve diffraction limit in this waveband. This is longer than UV-Vis wavelength by about 100-1,000, but such a telescope could be a pathfinder. The caveat of such an approach is that the sub-mm mirrors like *Herschel* need to be cooled to 85K, and then CTE mismatch between the coating and the substrate could lead to distortions that are beyond the ability of our design to correct. There is an alternative strategy in image correction: suppose that after correcting the primary figure, further image improvements are needed. Then the image could be further improved via a deformable secondary mirror (DM) [40]. The secondary could be of the classic design used to correct for atmospheric turbulence in ground-based adaptive optics systems.

The down side of a DM is that the smaller it is relative to the primary, the smaller the effective field of view (FOV). There is a simple rule of thumb is that the FOV decreases as the ratio of the diameter of the DM to the primary so that, for a 20 cm diameter DM and a 16m diameter primary, if the FOV of the primary is 1 degree, the resulting FOV of the primary plus DM is about 45".

Below is a detailed breakdown of the tasks.

Task 1: Analysis of MSM Coated Flat Membrane (6 months-NU)

One of the major tasks for Phase II is to demonstrate experimentally that we can apply a controlled deformation of a MSM coated membrane using magnetostriction. The goal will be to create deformations up to the order of 300 μm and to demonstrate that the deformation remains constant

on the level of a 1 μm over at least 1 week. First, a flat membrane will be used and, if time permits, a curved sample will be produced to measure the focusing ability of the corrected membrane. The substrate used for this test will be the low cost polyimide film Kapton® which can be molded to make a curved sample. If time permits, other optional substrates will be investigated.

Task 1.1: Decision about MSM Choice (2 months)

During Phase I two types of MSM have been selected; this choice will be refined and finalized to determine which magnetostrictive material will coat the samples. The amount of magnetostriction that is needed will be determined as part of this study.

Task 1.2: Production of Test Samples (1 month)

At least two samples of 5x5 cm will be made for each type of MSM in order to test the repeatability of the experiment. The simplest approach to deposit the MSM on the substrate is to use the system that is currently used at NU, which can sputter Terfenol-D and coat pieces that are 5 cm square. An alternative to this method is electroplating, but this option is too expensive for the team's budget.

Task 1.3: Evaluation of Test samples (3 months)

The sample will be mounted such that there is low in-plane stress, for instance, it can be clamped on all sides. Then it will be placed in a magnetic field (generated by permanent magnets or an electromagnet, or both in separate tests) that would cause a controlled deformation. Both the magnetic field and the surface shape will be measured. For the curved sample, a Shack-Hartmann test will be used to measure the accuracy of the optical figure. Due to the different CTEs of the materials, the samples will need to be put in a controlled thermal environment. The team thinks about maybe using a glove box equipped with a thermal control system. One unknown after Phase I is the time during which the membrane can hold the shape induced by magnetostriction. After being exposed to the magnetic field, the sample will be put at rest and its shape will be measured after 1.5, 5, and 7 days. This test can be repeated as needed.

Task 2: Simulation of Membrane Shape Correction Using Magnetostriction (1 year-NU)

The team needs to show that the deformations produced the magnetic field applied on the MSM can converge to the desired shape for the membrane and eventually to an improved reflected image.

Task 2.1: Investigation of Feedback Loop Controller (8 months)

The team will develop the ability to cause deformations in specific locations on the flat membrane in a non-interfering manner. In other words demonstrate that deformations at locations (call them A and B) about 1 cm apart can be produced such that the net deformations at A and B both have

the desired value. To carry out this task the team can use deformable mirror software [6][7][8] along with measurements made via lasers positioning systems such as [9] or as in an adaptive optics laboratory demonstration kit for deformable optics such at ThorLabs[10] in order to demonstrate that the figure can be improved using our approach.

Task 2.2: Simulation of Image Improvement (4 months)

After simulating the modifications in the membrane induced by magnetostriction, the results of Task 2.1 can be translated in terms of resulting image accuracy. Two types of image simulations will be done: first, using the size of the deflections obtained during the experiments of Task 1, and, second, using half the maximal deflection that is necessary to correct the post-deployment RMS error. This task can be linked to Task 3.4 by determining the length scales of the corrections that must be produced versus deployment ability.

Task 3: Verification of Deployment Methodology (18 months-UIUC)

Another major task of Phase II will be to demonstrate that the two deployment mechanisms selected during Phase I lead to a good enough post deployment surface accuracy. The aim is to prove that the RMS error of the deployed membrane can be corrected using magnetic write heads and magnetostriction. The targeted goal is to get an RMS error of about 100 μm.

Task 3.1: Design of Deployment Ground Test (6 months)

The flexible reflector and the self-deployable shell selected during Phase I require two different deployment mechanisms. The first one is slowly controlled by heating an elastic memory composite, while, for the second design, the deployment lasts only 2s. Hence, the team at UIUC will need to design two different procedures to test experimentally the deployment mechanisms. Another issue to tackle is how to measure the surface accuracy of the post-deployment shape of the membrane. An indirect method like the Shack-Hartmann test or photogrammetry techniques can be used to measure the surface shape before and after deployment.

Task 3.2: Fabrication of Deployment Structures (3 months)

Two models will be manufactured, one for each design. These models will be scaled down compared to the desired 16-m diameter APERTURE primary; and they will probably be about 30 cm to keep material costs low and to accommodate available lab space.

[6] www.mathworks.com/matlabcentral/fileexchange/33330-zernikecalc?s_tid=srchtitle
[7] www.openchannelsoftware.com/projects/PROPER
[8] www.okotech.com/mrfit
[9] resources.renishaw.com/en/details/data-sheet-rle-system-performance--33411
[10] www.thorlabs.com/newgrouppage9.cfm?objectgroup_id=3208

Task 3.3: Evaluation of Deployment Method (3 months)

After deploying the folded structures, the two deployments will be evaluated using the measured RMS error of the post-deployment shape. A cloth or thin film of nearly identical flexibility properties to the MSM covered membrane will be used as the primary mirror. This approach will be utilized to lower test cost and to allow the deployment tests to occur independently of the MSM coated membrane tests. The deployment test will be done several times in order to determine the repeatability of each approach.

Task 3.4: Analysis of Test Results (6 months)

The two deployment designs will be compared according to the following criteria: resulting RMS error, repeatability, stowed volume efficiency, stability, weight and cost.

Task 4: Further Investigations and Design of Full-Concept Demonstrations (6 months-UIUC)

Tasks 1-3 begin to answer the questions surrounding the APERTURE concept introduced earlier in this section. This information will enable the updating of the mission concept. However, further investigation will be required to fully answer the questions after Phase II. An on-orbit demonstration of the APERTURE concept presents the comprehensive next step in this effort.

Task 4.1: Refinement of Mission Concept (1 month)

Several steps will be undertaken to update the full mission concept. First, the utilization of a magnetic read and write head instead of just a write head will be considered. Two designs have been identified for the magnetic write head. Additionally, an updated concept of operations (ConOps) will be constructed using the results from Tasks 1, 2 and 3 and a selected concept for the magnetic write head system. A preliminary study will be done to compare the assets and drawbacks of in-orbit versus ground demonstrations.

Task 4.2: Design of an On-Orbit or Ground Demonstration Mission (5 months)

Depending on the result of Task 4.1, the design of an on-orbit or a ground demonstration will be initiated. A CubeSat mission would provide a dedicated, independent, on-orbit platform for evaluating the concept. UIUC will leverage their considerable experience designing and constructing several flight CubeSats as well as performing CubeSat mission concept studies (including for JPL) to design a CubeSat scale APERTURE demonstration payload and its corresponding mission. The demonstration design concept will be matured to the degree that it could be enacted after Phase II.

Task 5: Reporting and meeting

Progress reports will be done every 3 months, the team will also participate to the midterm review and will deliver a final report along with annual key enabling technologies reports. The PI Prof. Ulmer will attend to the NIAC symposiums.

7 Summary and Conclusions

In summary, astronomical as well as Earth observing applications of the future are counting on larger aperture telescopes than are currently available. Several groups have been working on the topic of enabling large (about 16-m diameter) UV-Vis telescopes for many years. The unique feature of our concept is that magnetic films are used rather than electrostatic films or piezo-electrostatic pads. Our magnetic film concept allows for contiguous correction along the surface, does not require a hard wire connection, and does not require continuous external application of the field. There are many unknowns related to the initial accuracy of the deployed figure prior to the magnetic write head corrections. The length scale over which the corrections need to be applied is also of concern. For, although approximately mm length scale corrections can be made with the MSM plus write head technology, the number of ≈ 1 mm² patches in a 16 m diameter mirror is too large to contemplate applying individual corrections to each individual patch. However, deployment strategies and the materials available continue to evolve, in particular shape memory composites (SMCs) [34] or alloys (SMAs) [41], such that at this time we see no show-stoppers for this concept. Furthermore, the ability to tune deformations down to much (factors of 10-100) smaller ($\approx$ μm) scale opens the futuristic possibility of improving the figure well beyond Strehl values of 90%.

8 Publications, Conferences and Patents

8.1 Publications and Conferences

This final report will be made available as a NIAC report in the public domain. In addition, we submitted the following article:

- M. P. Ulmer, V. L. Coverstone, J. Cao, *et al.*, "APERTURE, a Large Telescope using Magnetostriction for Post Deployment Corrections", special volume *Future Large-Aperture Ultraviolet/Optical/Infrared Space Observatory*, Journal of Astronomical Telescopes, Instruments, and Systems (JATIS), October-December 2016.

- M. P. Ulmer, V. L. Coverstone, J. Cao, *et al.*, "APERTURE, a large telescope using magnetostriction for post deployment corrections, an update", *in Proc. SPIE Astronomical Telescopes + Instrumentation, in Edinburgh, UK, 26 June – 1 July 2016*

We plan to participate in the following conference by attending and by giving an oral presentation at:

- SPIE Astronomical Telescopes + Instrumentation, in Edinburgh, UK, 26 June – 1 July 2016.

8.2 Patents

No patents have yet resulted from this project.

9 Contacts with experts in at NASA, NIST and Northrup Grumman

It is always useful to garner the input from experts in the field. Thus as part of this program we have established contacts who have graciously given time to consulted with us already. Furthermore we believe that those use names below that are underlined will be Phase II consultants. These are going from the East to West, general area of expertise in parentheses:

- Ron Shiri of GSFC (Space Optics)
- Santo Padula, II of NASA-Glen Research Center (Shape Memory Alloys)
- David Pappas of NIST Boulder (Magnetic Read-Write heads)
- C. Steve Arnold of Seagate (Magnetic Read-Write heads)
- Marco Quadrelli of JPL (Space Optics, NIAC Phase II Fellow)
- Geoff Marks of Northrup Grumman (Space Optics, AstroMesh)
- Ron Polidan of Northrup Grumman (Space Optics, JWST, Chandra)

10 Acknowledgments

This work was supported in part by a NASA NIAC grant number NNX15AL89G. We gratefully recognize many of the people who have given us input and support: Dr. G. Pareschi who introduced us to Dr. C. Joshi who introduced us to MSM films and their applications; Drs. X. Wang, Y. Yao, C. Liu who carried out MSM film coatings and the related measurements and modeling of deformation on glass; Drs. C. S. Arnold and D. Pappas for input on magnetic write heads, and Dr. S. Padula regarding SMAs.

11 References

[1] M. Postman, T. Brown, K. Sembach, *et al.*, "Advanced Technology Large- Aperture Space Telescope: science drivers and technology developments," *Opti- cal Engineering* **51**, 011007–011007 (2012).

[2] H. P. Stahl, H. Thronson, S. Langhoff, *et al.*, "Potential astrophysics science mis- sions enabled by NASA's planned Ares V," in *UV/Optical/IR Space Telescopes: Innovative Technologies and Concepts IV*, *Society of Photo-Optical Instrumen- tation Engineers (SPIE) Conference Series* **7436**, 743607 (2009).

[3] C. F. Lillie, R. S. Polidan, and D. R. Dailey, "Key enabling technologies for the next generation of space telescopes," in *Space Telescopes and Instrumen- tation 2010: Optical, Infrared, and Millimeter Wave*, *Society of Photo-Optical Instrumentation Engineers (SPIE) Conference Series* **7731**, 773102 (2010).

[4] "Three newly designedtracking and data relay satellites to help replenish existing on-orbit fleet," Tech. Rep. FS-2001-9-025-GSFC, NASA Goddard Space Flight Center (2001).

[5] M. W. Thomson, "Astromesh^{TM} deployable reflectors for Ku-and Ka-band com- mercial satellites," in *20th AIAA International Communication Satellite Systems Conference and Exhibit*, (2002).

[6] J. R. Hill, K. W. Wang, H. Fang, *et al.*, "Actuator grouping optimization on flexible space reflectors," in *Proceedings of SPIE - The International Society for Optical Engineering*, **7977** (2011).

[7] "Replicated diffractive optics, moire." http://www.ballaerospace.com/page. jsp?page=259. Accessed: 2015-01-26.

[8] S. E. Kendrick, R. Linfield, and D. Ebbets, "Optical requirements for a Ter- restrial Planet Finder optical coronagraph primary mirror," in *Techniques and Instrumentation for Detection of Exoplanets*, D. R. Coulter, Ed., **5170**, 13–24 (2003).

[9] B. D. Cullity and C. D. Graham, *Introduction to magnetic materials*, John Wiley & Sons, Inc., Hoboken, New Jersey (2009).

[10] J. Liu, C. Jiang, and H. Xu, "Giant magnetostrictive materials," *Science China Technological Sciences* **55**(5), 1319–1326 (2012).

[11] M. P. Ulmer, X. Wang, P. Knapp, *et al.*, "Comparisons of the deflections of magnetically smart films on alloy of NiCo and glass substrates," in *Adaptive X-Ray Optics III*, *Society of Photo-Optical Instrumentation Engineers (SPIE) Conference Series* **9208**, 920808 (2014).

[12] X. Wang, P. Knapp, S. Vaynman, *et al.*, "Experimental study and analytical model of deformation of magnetostrictive films as applied to mirrors for x-ray space telescopes," *Appl. Opt.* **53**, 6256–6267 (2014).

[13] X. Wang, Y. Yao, J. Cao, *et al.*, "Investigation of magnetically smart films applied to correct the surface profile of light weight X-ray optics in two directions," in *Society of Photo-Optical Instrumentation Engineers (SPIE) Conference Series*, *Society of Photo-Optical Instrumentation Engineers (SPIE) Conference Series* **9603**, 96031O (2015).

[14] A. Olabi, A.R. Grunwald, "Design and applications of magnetostrictive materials," *Materials and Design* **29** (2008).

[15] J. H.-G. Ng, P. M. Record, X. Shang, *et al.*, "Optimised co-electrodeposition of fe???ga alloys for maximum magnetostriction effect," *Sensors and Actuators A: Physical* **223**, 91 – 96 (2015).

[16] R. Mishra and E. J. Podlaha, "Coupled Partial Current Density Behavior of Cobalt?Terbium Alloy Codeposition," *Journal of The Electrochemical Society* **153** (2006).

[17] A. Ludwig and E. Quandt, "Giant magnetostrictive thin films for applications in microelectromechanical systems (invited)," *Journal of Applied Physics* **87**, 4691–4695 (2000).

[18] S. Guan and B. J. Nelson, "Magnetic composite electroplating for depositing micromagnets," *Journal of microelectromechanical systems* **15**, 330–337 (2006).

[19] L. Engdahl, *Handbook of giant magnetostrictive materials,*, Academic Press, San Diego (2000).

[20] M. McCaig, *Permanent magnets in theory and practice / Malcolm McCaig*, Pentech Press London (1977).

[21] X. Wang, *Mechanics of Magnetostrictive Thin Film Deformation and its Application in Active X-Ray Optics*. PhD thesis, Northwestern University (2016).

Submitted in 2016.

[22] "Delta IV, Payload Planners Guide," tech. rep., United Launch Alliance (2007).

[23] J. Enders, Kas-Danouche, W. Liao, *et al.*, "Design of a membrane aperture deployable structure," in *44th AIAA/ASME/ASCE/AHS Structures, Structural Dynamics, and Materials Conference, AIAA Conf. Proc.*, (Norfolk, Virginia) (2003).

[24] J. Domber and L. Peterson, "Implications of material microyield for gossamer optical reflectors," in *43rd AIAA/ASME/ASCE/AHS/ASC Structures, Struc- tural Dynamics, and Materials Conference*, American Institute of Aeronautics and Astronautics (AIAA) (2002).

[25] J. H. Li, X. X. Gao, J. Zhu, *et al.*, "Ductility, texture and large magnetostriction of fe-ga-based sheets," *Scripta Materialia* **63**(2), 246–249 (2010).

[26] P. N. Keller, M. S. Lake, D. Codell, *et al.*, "Development of elastic memory composite stiffeners for a flexible precision reflector," in *Collection of Technical Papers - AIAA/ASME/ASCE/AHS/ASC Structures, Structural Dynamics and Materials Conference*, **10**, 6984–6994 (2006).

[27] O. Soykasap, S. Karakaya, and E. Kaplan, "Self-deploying composite shell reflector antenna for ku-band missions: 1.5 m diameter demonstrator," in *RAST 2013 - Proceedings of 6th International Conference on Recent Advances in Space Technologies*, 631–636 (2013).

[28] O. Soykasap, S. Karakaya, A. Gayretli, *et al.*, "Preliminary design of deployable flexible shell reflector of an x-band satellite payload," in *2nd AIAA Spacecraft Structures Conference*, (2015).

[29] K. Hearon, P. Singhal, J. Horn, *et al.*, "Porous Shape Memory Polymers," *Polymer reviews (Philadelphia, Pa.)* **53**, 41–75 (2013).

[30] P. Stanley, "JWST Mission Operations Concept Document," tech. rep., Space Telescope Science Institute (2006).

[31] W. Larson and J. Wertz, *Space mission analysis and design*, Space technology library, Microcosm (1992).

[32] S. N. Williams and V. Coverstone-Carroll, "Benefits of solar electric propulsion for the next generation of planetary exploration missions," *Journal of the Astronautical Sciences* **45**(2), 143–159 (1997).

[33] J. Gal-Edd and E. Luers, "James webb space telescope ka-band trade," (2004).

[34] S. J. Varlese, M. P. Ulmer, J. Hermiller, *et al.*, "Performance characterization of a shape memory composite mirror," in *UV/Optical/IR Space Telescopes: Innova- tive Technologies and Concepts II*, H. A. MacEwen, Ed., *Society of Photo-Optical Instrumentation Engineers (SPIE) Conference Series* **5899**, 331–339 (2005).

[35] J. S. Knight, D. S. Acton, P. Lightsey, *et al.*, "Observatory alignment of the James Webb Space Telescope," in *Space Telescopes and Instrumentation 2012: Optical, Infrared, and Millimeter Wave, Society of Photo-Optical Instrumenta- tion Engineers (SPIE) Conference Series* **8442**, 84422C (2012).

[36] M. B. Quadrelli, L. J. Wood, J. E. Riedel, *et al.*, "Guidance, Navigation, and Control Technology Assessment for Future Planetary Science Missions," *Journal of Guidance Control Dynamics* **38**, 1165–1186 (2015).

[37] *Optical wavefront Sensors (Shack-Hartmann), WFS Series, Operation Manual* (2015).

[38] D. R. Neal, P. Pulaski, T. D. Raymond, *et al.*, "Testing highly aberrated large optics with a shack-hartmann wavefront sensor," in *Proceedings of SPIE - The International Society for Optical Engineering*, **5162**, 129–138 (2003).

[39] G. L. Pilbratt, J. R. Riedinger, T. Passvogel, *et al.*, "Herschel space observatory: An esa facility for far-infrared and submillimetre astronomy," *Astronomy and Astrophysics* **518** (2010).

[40] "The adaptive secondary mirror for the vlt." http://www.eso.org/sci/facilities/develop/ao/sys/dsm.html. Accessed: 2015-01-29.

[41] S. Padula, S. Qiu, D. Gaydosh, *et al.*, "Effect of Upper-Cycle Temperature on the Load-Biased, Strain-Temperature Response of NiTi," *Metallurgical and Materials Transactions A* **43**, 4610–4621 (2012).